Communications in Nonlinear Science and Numerical Simulation 115 (2022) 106789

Contents lists available at ScienceDirect

Communications in Nonlinear Science and Numerical Simulation

journal homepage: www.elsevier.com/locate/cnsns

Research paper

Equilibrium validation for triblock copolymers via inverse norm bounds for fourth-order elliptic operators

Peter Rizzi *, Evelyn Sander, Thomas Wanner

Department of Mathematical Sciences, George Mason University, Fairfax, VA 22030, USA

ARTICLE INFO

Article history:
Received 20 March 2022
Received in revised form 18 July 2022
Accepted 1 August 2022
Available online 4 August 2022

Dataset link: math.gmu.edu/~wanner/

MSC:
primary 37G15
37M20
65G20
65P30
secondary 37B35
37C70
65G30

Keywords:
Block copolymers
Ohta–Kawasaki equation
Operator norm bound
Computer-assisted proofs
Interval arithmetic
Rigorous validation
Bifurcations
Equilibrium structure

ABSTRACT

Block copolymers play an important role in materials sciences and have found widespread use in many applications. From a mathematical perspective, they are governed by a nonlinear fourth-order partial differential equation which is a suitable gradient of the Ohta–Kawasaki energy. While the equilibrium states associated with this equation are of central importance for the description of the dynamics of block copolymers, their mathematical study remains challenging. In the current paper, we develop computer-assisted proof methods which can be used to study equilibrium solutions in block copolymers consisting of more than two monomer chains, with a focus on triblock copolymers. This is achieved by establishing a computer-assisted proof technique for bounding the norm of the inverses of certain fourth-order elliptic operators, in combination with an application of a constructive version of the implicit function theorem. While these results are only applied to the triblock copolymer case, the obtained norm estimates can also be directly used in other contexts such as the rigorous verification of bifurcation points, or pseudo-arclength continuation in fourth-order parabolic problems.

1. Introduction

Block copolymers are materials formed from a number of different polymer molecules which are connected together in polymer chains. By combining monomers with different physical properties, one can create materials with completely new properties. For example, thermoplastic elastomers are a type of diblock copolymer, which combine rubbery monomers, such as polybutadiene or polyisoprene, with glassy hard monomers, such as polystyrene. Based on these two competing properties, one obtains a compound material that can be molded at high temperatures, but behaves as a rubber at low temperatures. Such block copolymers are used in a number of commercial applications, such as in sealants, gasket materials, hotmelt adhesives, rubber bands, toy products, shoe soles, and even in road paving and roofing applications.

* Corresponding author.
E-mail address: prizzi@gmu.edu (P. Rizzi).

https://doi.org/10.1016/j.cnsns.2022.106789
1007-5704/

From a physical perspective, the study of diblock copolymers, which consist of exactly two different monomers, was initiated by Ohta and Kawasaki [1]. They proposed a free energy functional for the description of such systems, which extends the standard van der Waals free energy functional [2] by a nonlocal term. This addition models the competition between both long-range and short-range forces in the material, and it causes *microphase separation*, which in turn results in pattern formation on a mesoscopic scale. The observed pattern morphology is extremely rich, and one can observe complicated microstructure such as gyroids, perforated layers, and more. See for example [3] and the references therein.

Mathematical studies of diblock copolymers have focused on dynamical aspects of these materials. As already developed in [1], one can associate gradient dynamics with the Ohta–Kawasaki energy functional, which leads to a fourth-order nonlinear parabolic partial differential equation. Being dissipative, this equation has a global attractor, and its structure is responsible for the long-term dynamics of the model [4,5]. Of particular interest is the set of equilibrium states of the diblock copolymer model. While the numerous local and global energy minimizers of the Ohta–Kawasaki energy describe potential long-term limits, even the saddles of the energy play an important role in the selection of specific stable states [6–10]. There have been a number of studies which proved the existence of equilibrium solutions of certain types, see for example [4,11–14] and the references therein. More recently, computer-assisted proofs have been used to obtain mathematically rigorous results concerning the equilibrium structure, see for example [15–19].

With the present paper, we start a study of equilibrium solutions for block copolymers consisting of more than two monomers. For the sake of specificity, we focus on the case of triblock copolymers, which were first discussed in [20], and whose rich variety of steady state microstructures has been illustrated in [21,22]. Such systems have only recently become the subject of mathematical studies, see for example [23,24]. For the present paper, we study the triblock copolymer system given by

$$\begin{aligned} \frac{\partial u_1}{\partial t} &= -\Delta\left(\varepsilon^2 \Delta u_1 + f_1(u_1,u_2)\right) - \sigma\,(u_1-\mu_1)\ , \\ \frac{\partial u_2}{\partial t} &= -\Delta\left(\varepsilon^2 \Delta u_2 + f_2(u_1,u_2)\right) - \sigma\,(u_2-\mu_2)\ , \\ & u_1+u_2+u_3 \;=\; 1. \end{aligned} \tag{1}$$

In this system, the functions $u_1, u_2, u_3 \colon \Omega \;\to\; \mathbb{R}$ describe the three monomer components. More precisely, values between 0 and 1 of $u_i(t,x)$ indicate that at time t and location $x \in \Omega$ the ith monomer has concentration $u_i(t,x)$. Since the above model is of phase-field type, the function values of the u_i may not actually lie between 0 and 1, but they generally stay close to this interval, and we interpret negative values or values larger than one as being equal to concentrations of 0 or 1 in the physical system, respectively. This is similar to the phase variables considered for example in the Allen–Cahn or Cahn–Hilliard models, up to an affine transformation. The above system of equations has to be satisfied in a bounded domain $\Omega \subset \mathbb{R}^d$ for $d = 1, 2, 3$, where for the purposes of this paper we restrict ourselves to the unit cube $\Omega = (0,1)^d$. In addition, we consider (1) subject to homogeneous Neumann boundary conditions for all u_i and Δu_i, the small parameter $\varepsilon > 0$ models interaction length, and $\sigma \geq 0$ represents the polymer length scale, just as in the diblock copolymer case [16]. If we further define $\mu_3 = 1 - \mu_1 - \mu_2$, then the three constants μ_i have to be nonnegative, and they represent the total mass of the three involved monomers in the sense that

$$\frac{1}{|\Omega|}\int_\Omega u_i(t,x)\,dx \;=\; \mu_i \qquad \text{for all} \qquad t \geq 0 \quad \text{and} \quad i = 1,2,3. \tag{2}$$

Finally, the functions f_1 and f_2 are suitable nonlinearities which are derived from the gradient of a triple-well potential and which will be described in more detail in our model derivation in the next section.

Our approach for establishing the existence of equilibrium solutions of the triblock copolymer system (1) subject to the mass constraints in (2) is based on the constructive implicit function theorem introduced in [25], combined with the rigorous Sobolev estimates of [26] and extends the approach used in [16] for the diblock copolymer case. More precisely, we use spectral approximations based on cosine series to find an approximate solution, and then have to establish the following three estimates:

- First of all, one has to determine the residual of the approximate solution, which in view of our use of a spectral approximation combined with polynomial nonlinearities, amounts to little more than evaluating a finite sum in interval arithmetic.
- Next, one needs local Lipschitz bounds on the Fréchet derivative of (1) at the approximate solution, which can easily be obtained using the above-mentioned Sobolev embedding results.
- The last and most difficult step is to obtain a rigorous bound on the operator norm of the inverse of the Fréchet derivative of (1) at the approximate solution. While in principle this will be accomplished as in [16], the specifics must be adapted to the current situation. This step is definitely the most elaborate part of the proof.

Once the above three tasks have been completed, one obtains computer-assisted proofs for small solution branches of equilibrium solutions of (1), similar to [25, Theorem 5] and [16, Section 5].

The above approach has a couple of shortcomings. In particular, the direct use of the constructive implicit function theorem only provides small branch segments, as the theorem in its original form is not aligned to the actual tangent direction of the branch; see the discussion in [25]. Additionally, in order to follow a branch through a saddle–node

bifurcation or to directly verify of the existence of certain bifurcation points requires applying the constructive implicit function theorem to a suitable extended system. See for example [9,25,27,28]. In all of these cases, one has to study different extensions of the system (1). In its current form, for each of these applications the elaborate third step above has to be redone.

One of the main contributions of the current paper is the development of a flexible general framework such that this reassembly for each application is not necessary. Namely, we derive the norm estimate on the inverse operator right away for a sufficiently large class of linear systems, such that we can easily reuse already calculated results for a variety of different extended systems. More precisely, the central part of this paper is devoted to obtaining such estimates for linear operators L acting on $m \in \mathbb{N}_0$ scalar parameters $\eta_1, \dots, \eta_m$ and on $n \in \mathbb{N}$ functions $v_k : \Omega \to \mathbb{R}$ in such a way that the first m components of L are given by the scalars

$$\sum_{i=1}^{m} \alpha_{ki}\eta_i + \sum_{j=1}^{n} l_{kj}(v_j) \qquad \text{for} \qquad k = 1, \dots, m\,, \tag{3}$$

and the next n components of L are given by the functions

$$-\beta_k \Delta^2 v_k - \sum_{i=1}^{m} b_{ki}\eta_i - \Delta \sum_{j=1}^{n} c_{kj} v_j - \sum_{j=1}^{n} \gamma_{kj} v_j \qquad \text{for} \qquad k = 1, \dots, n. \tag{4}$$

In these formulas, the variables α_{ki}, $\beta_k > 0$, and γ_{kj} refer to real constants, while b_{ki} and c_{kj} denote suitably smooth real-valued functions defined on Ω, and l_{kj} denotes a bounded linear functional on the ambient space for v_j with Riesz representative in a suitable finite dimensional subspace.

At first glance, the generality of the linear operators defined in (3) and (4) might seem exaggerated, given that the main application of this paper is the establishment of certain triblock copolymer microstructures. In fact, however, the above generality allows for a number of direct applications:

- An immediate application is the study of pitchfork bifurcation points in the diblock copolymer model which are induced by symmetry-breaking based on a cyclic group action [28]. While these results answer an open question posed in [9], the latter paper was based on the radii polynomial approach, and one would have to adapt the estimates for every group order to obtain a computer-assisted proof. The estimates of the present paper apply directly and without change.
- We can extend the initial study of triblock copolymers in this paper to a more systematic study of their bifurcation diagrams using rigorous pseudo-arclength continuation, and thereby shed some light on the creation of bubble assemblies [24].
- The norm bound estimate can be used to obtain rigorous results on double and quadruple bubbles in multi-component metallic alloys, as modeled by Cahn–Morral systems [29]. So far, only numerical results have been obtained in [30].
- More generally, our construction opens the door to a more detailed study of the bifurcation structure of the celebrated Cahn–Hilliard model on higher-dimensional domains [31,32], including pseudo-arclength continuation, bifurcation point verification, and continuation of bifurcation points in a two-parameter setting.

The above list is not meant to be exhaustive, but rather to justify the extra effort which is necessary to study the linear operator defined in (3) and (4). For the sake of keeping the current paper from becoming too long, we will address these applications in future work.

The remainder of the paper is organized as follows. Section 2 is devoted to our preliminary study of triblock copolymers. In addition to deriving the model and describing its basic stability as a function of the mass vector, we also describe how a constructive version of the implicit function theorem can be used to obtain computer-assisted proofs for small branches of equilibrium solutions. The section closes with the presentation of specific computer-assisted proofs of a variety of observed microstructures. Section 3 introduces the functional-analytic framework for our computer-assisted equilibrium validation. In addition to recalling definitions and results from [16,26], we also derive the Lipschitz estimates which are necessary for the application of the constructive implicit function theorem. The remaining ingredient for the validation of the triblock copolymer stationary states is the derivation of the inverse norm bound, which is the subject of Section 4. Finally, Section 5 contains conclusions and future applications.

2. Validated triblock copolymer equilibria

Before diving into the more technical parts of the paper, we demonstrate how these results can be applied in the context of triblock copolymers. More precisely, in the present section we rigorously validate equilibria for the triblock copolymer model, by establishing intriguing patterns for a variety of different mass vectors. To our knowledge, this is the first computer-assisted result in this context.

To accomplish this, Section 2.1 briefly describes the derivation of the model from its energy functional, which is followed in Section 2.2 by a discussion of the stability of the homogeneous steady state and the creation of nontrivial

steady states via bifurcations from the homogeneous one. We then present the framework for our computer-assisted equilibrium validation in Section 2.3, which is based on a constructive version of the implicit function theorem. Finally, Section 2.4 contains sample computer-assisted existence proofs for equilibrium solutions, which are all based on the functional-analytic framework described in Section 3 and the main inverse norm bound derived in Section 4.

2.1. Derivation of the triblock copolymer model

The dynamics of triblock copolymers are dictated by their associated free energy as introduced in [20], which is given by

$$E_{\varepsilon,\sigma}[u] \;=\; \int_\Omega \left(\frac{\varepsilon^2}{2} \sum_{i=1}^{3} |\nabla u_i|^2 + F(u) + \frac{\sigma}{2} \sum_{i=1}^{3} \left| (-\Delta)^{-1/2} (u_i - \mu_i) \right|^2 \right) dx \,, \tag{5}$$

where $u = (u_1, u_2, u_3) \colon \Omega \to \mathbb{R}^3$ denotes a material state which satisfies $u_1 + u_2 + u_3 = 1$ throughout Ω, and F is the triple-well potential given by

$$F(u) = F(u_1, u_2, u_3) = \sum_{i=1}^{3} g(u_i) \qquad \text{with} \qquad g(s) = \frac{27 s^2 (1-s)^2}{4}. \tag{6}$$

This energy functional has global minima at the three points $(1, 0, 0)$, $(0, 1, 0)$, and $(0, 0, 1)$, which correspond to the three pure monomers. From this energy functional, one can derive several different gradient-like evolution equations if the function u also shows t-dependence. While the recent study [24] considered a standard $L^2(\Omega)$-gradient, which results in a nonlocal second-order evolution equation, we follow the standard procedure which in the two-component case leads to the Ohta–Kawasaki model. That is, we use the $H^{-1}(\Omega)$-gradient instead. This results in a local fourth-order partial differential equation, which exhibits a structure similar to the classical Cahn–Hilliard, Cahn–Morral, or Ohta–Kawasaki models.

In order to arrive at an evolution equation for the first two components u_1 and u_2 only, which respects the conservation of mass identity $u_1 + u_2 + u_3 = 1$ throughout Ω, we follow the procedure outlined in [29,33,34] for the Cahn–Morral case. For this, define the vector-valued function $u := (u_1, u_2, u_3) \colon \Omega \to \mathbb{R}^3$ and let $\mu = (\mu_1, \mu_2, \mu_3)$ be the vector of total masses of the three involved monomers, as defined in (2). In fact, we assume that the latter mass vector lies in the *Gibbs triangle* $\mathcal{G}$ defined as

$$\mathcal{G} := \left\{ \mu \in \mathbb{R}^3 \,:\, \sum_{i=1}^{3} \mu_i = 1 \quad \text{and} \quad \mu_i \geq 0 \quad \text{for} \quad i = 1, 2, 3 \right\} .$$

By computing the $H^{-1}(\Omega)$-gradient of (5) as in [29,33,34], one can then associate the gradient dynamics given by

$$\begin{aligned} \frac{\partial u}{\partial t} \;&=\; -\Delta \left(\varepsilon^2 \Delta u + \bar{f}(u) \right) - \sigma (u - \mu) \quad \text{in} \quad \Omega \,, \\ \frac{\partial u}{\partial \nu} \;&=\; \frac{\partial \Delta u}{\partial \nu} \;=\; 0 \quad \text{on} \quad \partial\Omega \,, \end{aligned} \tag{7}$$

where ν denotes the unit outward normal vector to the boundary $\partial\Omega$. We would like to point out that while at first glance this equation appears to be exactly the diblock copolymer model, it is in fact a system of equations for the vector-valued function u, i.e., for all $t \geq 0$ and arbitrary $x \in \Omega$ we have $u(t, x) \in \mathbb{R}^3$. The nonlinearity $\bar{f} \colon \mathbb{R}^3 \to \mathbb{R}^3$ is given by

$$\bar{f}(u) = -P \nabla F(u) \,, \qquad \text{where} \qquad Pv = v - \frac{v \cdot \mathbf{e}}{|\mathbf{e}|^2} \mathbf{e} \quad \text{and} \quad \mathbf{e} = (1, 1, 1) \,.$$

This form of the nonlinearity ensures that the right-hand side of (7) is pointwise orthogonal to the vector $\mathbf{e}$, and therefore the evolution of this partial differential equation leaves the affine space $u_1 + u_2 + u_3 = 1$ pointwise invariant. One can therefore consider the first two equations of the evolution equation (7) only, where we replace u_3 by $1 - u_1 - u_2$. Thus, we finally obtain the equation stated in (1), where the nonlinearities f_1 and f_2 are given by

$$\begin{aligned} f_1(u_1, u_2) \;&=\; \bar{f}_1(u_1, u_2, 1 - u_1 - u_2) \;=\; \frac{-2g'(u_1) + g'(u_2) + g'(1 - u_1 - u_2)}{3} \,, \\ f_2(u_1, u_2) \;&=\; \bar{f}_2(u_1, u_2, 1 - u_1 - u_2) \;=\; \frac{g'(u_1) - 2g'(u_2) + g'(1 - u_1 - u_2)}{3} \,, \end{aligned}$$

where g was defined in (6).

In the present paper, we will study the set of equilibrium states of the system (1), i.e., we set the right-hand sides in the partial differential equations equal to zero, which in turn gives the fourth-order elliptic nonlinear system

$$\begin{aligned} -\Delta \left(\varepsilon^2 \Delta u_1 + f_1(u_1, u_2) \right) - \sigma \, (u_1 - \mu_1) \;&=\; 0 \,, \qquad \frac{1}{|\Omega|} \int_\Omega u_1 \, dx \;=\; \mu_1 \,, \\ -\Delta \left(\varepsilon^2 \Delta u_2 + f_2(u_1, u_2) \right) - \sigma \, (u_2 - \mu_2) \;&=\; 0 \,, \qquad \frac{1}{|\Omega|} \int_\Omega u_2 \, dx \;=\; \mu_2 \,, \end{aligned} \tag{8}$$

subject to homogeneous Neumann boundary conditions for u_i and Δu_i, for $i = 1, 2$.

2.2. Stability of the homogeneous steady state

One can easily see that the equilibrium problem (8) for the triblock copolymer equation has the spatially constant solution (μ_1, μ_2), whenever we have $\mu = (\mu_1, \mu_2, \mu_3) \in \mathcal{G}$. Thus, one can hope to find nontrivial equilibria through path-following from this homogeneous steady state as the parameter ε is varied. Since one can easily see that for large values of ε the homogeneous state is stable (see also the discussion below), we need to focus on mass vectors for which this steady state becomes unstable as ε decreases.

More generally, suppose now that $u_1, u_2 : \Omega \to \mathbb{R}$ denotes a solution of the system (8), i.e., the functions u_1, u_2, and $u_3 = 1 - u_1 - u_2$ are an equilibrium for the triblock copolymer equation (1). In order to understand the stability of this steady state one has to consider the linearization given by

$$\begin{aligned} \frac{\partial v_1}{\partial t} &= -\Delta\left(\varepsilon^2 \Delta v_1 - \frac{2}{3} g''(u_1) v_1 + \frac{1}{3} g''(u_2) v_2 - \frac{1}{3} g''(u_3)(v_1 + v_2)\right) - \sigma v_1 \,, \\ \frac{\partial v_2}{\partial t} &= -\Delta\left(\varepsilon^2 \Delta v_2 + \frac{1}{3} g''(u_1) v_1 - \frac{2}{3} g''(u_2) v_2 - \frac{1}{3} g''(u_3)(v_1 + v_2)\right) - \sigma v_2 \,, \end{aligned} \tag{9}$$

or, more precisely, the spectrum of the linear elliptic operator induced by its right-hand side. For the homogeneous case this linearization simplifies to the linear partial differential equation

$$\frac{\partial}{\partial t}\begin{pmatrix} v_1 \\ v_2 \end{pmatrix} = -\Delta\left(\varepsilon^2 \Delta \begin{pmatrix} v_1 \\ v_2 \end{pmatrix} + M \begin{pmatrix} v_1 \\ v_2 \end{pmatrix}\right) - \sigma \begin{pmatrix} v_1 \\ v_2 \end{pmatrix} \,, \tag{10}$$

where the matrix $M \in \mathbb{R}^{2\times 2}$ is defined as

$$M = \frac{1}{3}\begin{pmatrix} -2g''(\mu_1) & g''(\mu_2) \\ g''(\mu_1) & -2g''(\mu_2) \end{pmatrix} - \frac{1}{3} g''(1 - \mu_1 - \mu_2) \begin{pmatrix} 1 & 1 \\ 1 & 1 \end{pmatrix}. \tag{11}$$

This linearization is considered subject to homogeneous Neumann boundary conditions as before, and in addition, with the homogeneous integral constraints $\int_\Omega v_1 \, dx = \int_\Omega v_2 \, dx = 0$. Its stability is the subject of the next lemma.

Lemma 2.1 (*Stability of the Homogeneous State*)**.** *Let $\mu \in \mathcal{G}$ denote an arbitrary mass vector in the Gibbs triangle, and consider the linearization of the triblock copolymer model (1) at this homogeneous state, as given in (10) and (11) above. Then the matrix M is diagonalizable, i.e., we can find two eigenvalues $\nu_1, \nu_2 \in \mathbb{R}$ and eigenvectors $p_1, p_2 \in \mathbb{R}^2$ such that*

$$Mp_1 = \nu_1 p_1 \quad \text{and} \quad Mp_2 = \nu_2 p_2 \,, \quad \text{as well as} \quad \nu_1 \geq \nu_2. \tag{12}$$

Furthermore, if the eigenvalues of the negative Laplacian subject to homogeneous Neumann boundary conditions and zero mass constraint on Ω are given by $0 < \kappa_1 \leq \kappa_2 \leq \ldots \to \infty$, and the associated eigenfunctions φ_k satisfy

$$-\Delta \varphi_k = \kappa_k \varphi_k \quad \text{on } \Omega \qquad \text{and} \qquad \frac{\partial \varphi_k}{\partial \nu} = 0 \quad \text{on } \partial\Omega \,, \tag{13}$$

then the following hold:

(a) For every $j = 1, 2$ and $k \in \mathbb{N}$ the vector $p_j \varphi_k$ of functions is an eigenfunction of the right-hand side of (10) with associated eigenvalue

$$\lambda_{j,k} = \kappa_k \left(\nu_j - \varepsilon^2 \kappa_k\right) - \sigma. \tag{14}$$

Furthermore, the spectrum of the operator given by the right-hand side of (10) consists precisely of these eigenvalues $\lambda_{j,k}$ for $j = 1, 2$ and $k \in \mathbb{N}$.

(b) If the inequality $\nu_2 \leq \nu_1 \leq 0$ holds, then the homogeneous equilibrium μ of (1) is stable for all values $\varepsilon > 0$. On the other hand, if we have $\nu_1 > 0$, then the homogeneous state is unstable for all sufficiently small $\varepsilon > 0$.

Proof. It is elementary to show that if we write $\mu_3 = 1 - \mu_1 - \mu_2$, then the characteristic polynomial of the matrix M has the discriminant

$$\frac{2}{9}\left(\left(g''(\mu_1) - g''(\mu_2)\right)^2 + \left(g''(\mu_2) - g''(\mu_3)\right)^2 + \left(g''(\mu_3) - g''(\mu_1)\right)^2\right) \geq 0 \,,$$

which is clearly nonnegative. Thus, the matrix M always has two real eigenvalues and associated real eigenvectors, i.e., we can assume that (12) is satisfied. But then one easily obtains that the pair of functions $\psi = p_j \varphi_k$ satisfies the identity $-\Delta(\varepsilon^2 \Delta \psi + M\psi) = \lambda_{j,k}\psi$, by applying (13) component-wise, in combination with (12). In addition, note that according to our construction the eigenfunctions $\{\varphi_k\}_{k\in\mathbb{N}}$ form a complete orthogonal set in the Hilbert space $X = \{w \in L^2(\Omega) : \int_\Omega w \, dx = 0\}$. Thus, the function pairs $p_j \varphi_k$ for $j = 1, 2$ and $k \in \mathbb{N}$ form a complete orthogonal set in $X \times X$, which immediately establishes *(a)*. Finally, the statements in *(b)* follow easily from the formula in (14) and the fact that $\kappa_k > 0$ for all $k \in \mathbb{N}$. This completes the proof of the lemma. □

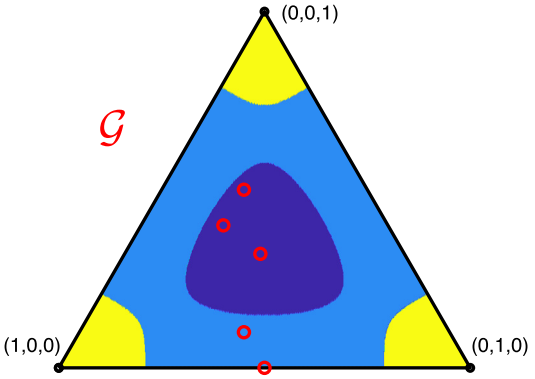

μ_1	μ_2	μ_3
0.30	0.20	0.50
0.40	0.20	0.40
0.35	0.33	0.32
0.50	0.40	0.10
0.50	0.50	0.00

Fig. 1. Stability regions for the homogeneous steady state of the triblock copolymer model (1) in the Gibbs triangle $\mathcal{G}$. For total mass vectors in the yellow regions the homogeneous state is stable, if the vector lies in either the light or dark blue areas, then the state is unstable for sufficiently small $\varepsilon > 0$. The dark blue region corresponds to $\nu_1 \geq \nu_2 > 0$, while the light blue region is for $\nu_1 > 0 \geq \nu_2$ in (12). The five red dots indicate mass vectors at which we validated nontrivial solutions, and the associated mass values are listed in the table. Figs. 3 and 5–7 have μ values in the dark blue region, whereas Figs. 2 and 4 have values of μ in the light blue region.

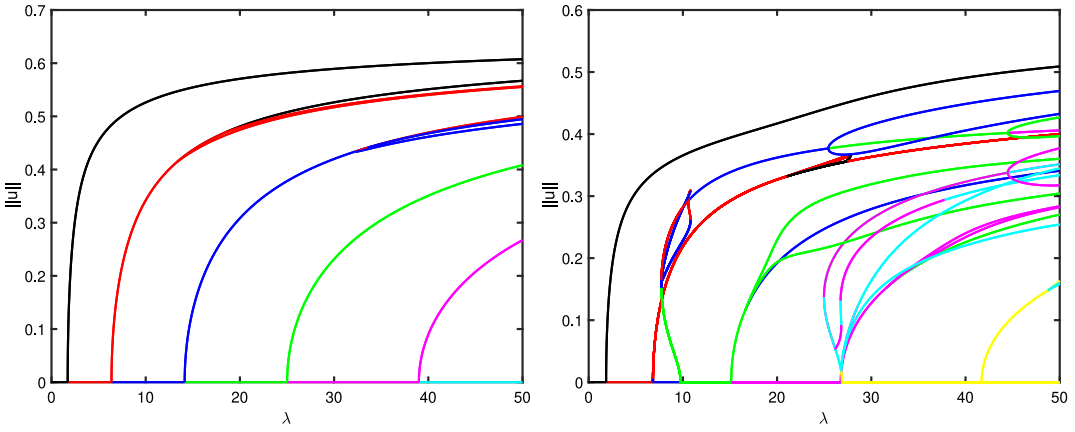

Fig. 2. Sample numerically computed bifurcation diagrams for the triblock copolymer equilibrium solutions on the one-dimensional domain $\Omega = (0, 1)$. The parameters $\sigma = 6.0$ and on left $\mu = (0.5, 0.4, 0.1)$ and right $\mu = (0.4, 0.2, 0.4)$ are held fixed, while $\lambda = 1/\varepsilon^2$ is permitted to vary. The color coding represents the index of the equilibrium branch, with black, red, blue, green, and magenta corresponding to index 0, 1, 2, 3, and 4, respectively. Since $\mu_3 \approx 0$ in the left image, the diagram is qualitatively very similar to the one of the diblock copolymer equation shown in [8,9]. For the right image, since $\mu_3 \gg 0$, the diagram looks very different.

The stability of the homogeneous steady state $\mu = (\mu_1, \mu_2, \mu_3) \in \mathcal{G}$ is illustrated in Fig. 1. In this figure, yellow regions correspond to $\nu_2 \leq \nu_1 \leq 0$, i.e., in those regions the homogeneous state μ is stable for all $\varepsilon > 0$. On the other hand, the light blue region corresponds to the inequality $\nu_1 > 0 \geq \nu_2$, while the dark blue region is for $\nu_1 \geq \nu_2 > 0$. In both of these regions, the homogeneous state μ is unstable for all sufficiently small $\varepsilon > 0$, and one can hope to observe sudden phase separation in solutions of the triblock copolymer model originating nearby.

To explain this last comment in more detail, we introduce an abbreviation which will be used throughout the remainder of the paper. As mentioned in the previous paragraph, the stability of the homogeneous state in the blue regions of Fig. 1 changes for small enough values of ε, and in fact it is the limit $\varepsilon \to 0$ which leads to interesting nonhomogeneous stationary states. Uncovering these states will be accomplished by continuation techniques, and it is therefore more convenient to instead introduce the new parameter

$$\lambda = \frac{1}{\varepsilon^2}$$

which is then studied in the limit $\lambda \to \infty$. One can easily see that if we divide both sides of the linearized problem (9) by ε^2 and rescale time, the spectrum of the right-hand side for small $\lambda \approx 0$ is a small perturbation of the spectrum of the stable bi-Laplacian operator $-\Delta^2$. Now consider a homogeneous mass vector μ in one of the blue regions in Fig. 1. Then the stability of the associated homogeneous state has to change as λ increases, and standard results from bifurcation theory imply the appearance of nontrivial equilibrium solutions. This can be seen in Figs. 2 and 3, which contain sample numerically computed bifurcation diagrams for a few different mass vectors in the blue regions. The diagrams in Fig. 2 are

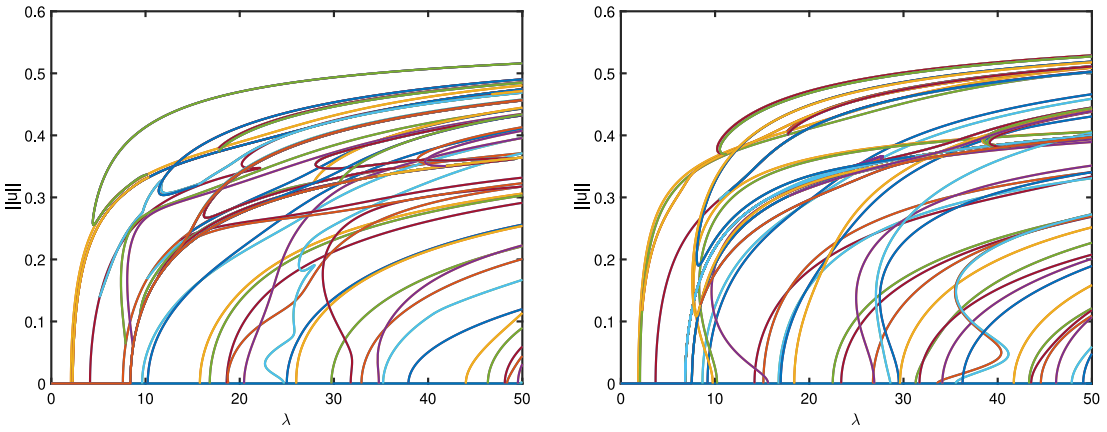

Fig. 3. Sample numerically computed triblock copolymer bifurcation diagrams for the two-dimensional domain $\Omega = (0, 1)^2$. In both figures, we have chosen $\sigma = 6.0$ and $\lambda = 1/\varepsilon^2$ varies. The left diagram is for mass vector $\mu = (0.3, 0.2, 0.5)$, while the right panel is for the vector $\mu = (0.4, 0.2, 0.4)$. These diagrams are not a complete set of all equilibrium solutions, but they give a sense of the vast array of possible solutions one can find.

for the triblock copolymer model on the one-dimensional domain $\Omega = (0, 1)$, while the ones in Fig. 3 are for $\Omega = (0, 1)^2$. Notice that all of these diagrams indicate the appearance of a multitude of nontrivial stationary states. Moreover, while their number seems manageable in the one-dimensional situation, this is no longer the case in space dimension two. In the remainder of this paper, we show how these numerically computed equilibrium solutions can be established rigorously.

2.3. Computer-assisted equilibrium validation

Our rigorous equilibrium validation is a significant extension of the constructive implicit function theorem approach which was first introduced in [19,25], and which was further refined in [16]. In the present subsection, we demonstrate how it can be adapted to the situation of the triblock copolymer model. Our goal is to prove the existence of stationary states for the triblock copolymer model on the domain $\Omega = (0, 1)^d$, where for the purposes of this paper we focus on $d = 1, 2$. Such equilibrium solutions satisfy the nonlinear elliptic system (8), which for our approach has to be slightly reformulated. Due to the involved mass constraints, we introduce the transformations

$$u_1 = \mu_1 + w_1 \qquad \text{and} \qquad u_2 = \mu_2 + w_2 \,.$$

Furthermore, as mentioned already at the end of the last subsection, rather than visualizing bifurcation diagrams in the $\varepsilon - (w_1, w_2)$-coordinate system and the small limit $\varepsilon \to 0$, which would imply that the equilibrium branches of interest become arbitrarily close together, we instead use the large continuation parameter $\lambda = 1/\varepsilon^2$. Thus instead of (8) we consider the transformed system

$$\begin{aligned} -\Delta\left(\Delta w_1 + \lambda f_1(\mu_1 + w_1, \mu_2 + w_2)\right) - \lambda\sigma w_1 &= 0\,, \qquad \int_\Omega w_1\,dx = 0\,, \\ -\Delta\left(\Delta w_2 + \lambda f_2(\mu_1 + w_1, \mu_2 + w_2)\right) - \lambda\sigma w_2 &= 0\,, \qquad \int_\Omega w_2\,dx = 0. \end{aligned} \tag{15}$$

The underlying basic function spaces are the following Sobolev spaces, where the subscript n indicates Neumann boundary conditions.

$$\bar{H}^2_n(\Omega) = \left\{ w \in H^2(\Omega) : \int_\Omega w\,dx = 0\,,\ \frac{\partial w}{\partial \nu} = 0 \text{ on } \partial\Omega \right\} \text{ and } \bar{H}^{-2}_n(\Omega) = \bar{H}^2_n(\Omega)^*. \tag{16}$$

Then the equilibrium system (15) can be written as the nonlinear zero finding problem

$$\mathcal{F}(\lambda, w) = 0 \qquad \text{for} \qquad \mathcal{F} : \mathbb{R} \times \mathcal{X} \to \mathcal{Y} \tag{17}$$

with

$$\mathcal{X} = \bar{H}^2_n(\Omega) \times \bar{H}^2_n(\Omega) \quad \text{and} \quad \mathcal{Y} = \bar{H}^{-2}_n(\Omega) \times \bar{H}^{-2}_n(\Omega)\,, \tag{18}$$

as well as

$$\begin{aligned} \mathcal{F}(\lambda, (w_1, w_2)) &= -\Delta(\Delta w + \lambda f(\mu + w)) - \lambda\sigma w \\ &= \begin{pmatrix} -\Delta\left(\Delta w_1 + \lambda f_1(\mu_1 + w_1, \mu_2 + w_2)\right) - \lambda\sigma w_1, \\ -\Delta\left(\Delta w_2 + \lambda f_2(\mu_1 + w_1, \mu_2 + w_2)\right) - \lambda\sigma w_2\,. \end{pmatrix} \end{aligned} \tag{19}$$

This system is solved using the constructive implicit function theorem presented in [25], which is based on similar results in [19,35]. We state this theorem below. For its application, one needs to establish the following four assumptions:

(H1) Assume that we have found a numerical approximation $(\lambda^*, w^*) \in \mathbb{R} \times \mathcal{X}$ of a solution of the system (17). Then one needs to find an explicit constant $\varrho > 0$ such that

$$\left\| \mathcal{F}(\lambda^*, w^*) \right\|_{\mathcal{Y}} \leq \varrho \ .$$

(H2) Assume that the Fréchet derivative $D_w \mathcal{F}(\lambda^*, w^*) \in \mathcal{L}(\mathcal{X}, \mathcal{Y})$ is invertible, and that its inverse $D_w \mathcal{F}(\lambda^*, w^*)^{-1} : \mathcal{Y} \to \mathcal{X}$ is bounded and satisfies the estimate

$$\left\| D_w \mathcal{F}(\lambda^*, w^*)^{-1} \right\|_{\mathcal{L}(\mathcal{Y},\mathcal{X})} \leq K \ ,$$

for some explicit constant $K > 0$, where $\| \cdot \|_{\mathcal{L}(\mathcal{Y},\mathcal{X})}$ denotes the operator norm in $\mathcal{L}(\mathcal{Y}, \mathcal{X})$.

(H3) There exist constants $L_1, L_2, \ell_w > 0$ and $\ell_\lambda \geq 0$ such that for all pairs $(\lambda, w) \in \mathbb{R} \times \mathcal{X}$ with $\|w - w^*\|_{\mathcal{X}} \leq \ell_w$ and $|\lambda - \lambda^*| \leq \ell_\lambda$ we have

$$\left\| D_w \mathcal{F}(\lambda, w) - D_w \mathcal{F}(\lambda^*, w^*) \right\|_{\mathcal{L}(\mathcal{X},\mathcal{Y})} \leq L_1 \left\| w - w^* \right\|_{\mathcal{X}} + L_2 \left| \lambda - \lambda^* \right| \ .$$

(H4) There exist constants $L_3, L_4 > 0$ such that for all $\lambda \in \mathbb{R}$ with $|\lambda - \lambda^*| \leq \ell_\lambda$ one has

$$\left\| D_\lambda \mathcal{F}(\lambda, w^*) \right\|_{\mathcal{Y}} \leq L_3 + L_4 \left| \lambda - \lambda^* \right| \ ,$$

where ℓ_λ is the constant from (H3).

The constructive implicit function theorem from [25] then takes the following form.

Theorem 2.2 (*Constructive Implicit Function Theorem*). *Let $\mathcal{X}$ and $\mathcal{Y}$ denote the Hilbert spaces defined in (18), and let $\mathcal{F} : \mathbb{R} \times \mathcal{X} \to \mathcal{Y}$ be defined as in (19). Furthermore, suppose that the pair $(\lambda^*, w^*) \in \mathbb{R} \times \mathcal{X}$ satisfies hypotheses (H1) through (H4). Finally, suppose that*

$$4K^2 \varrho L_1 < 1 \qquad \text{and} \qquad 2K\varrho < \ell_w. \tag{20}$$

Then there exist pairs of constants $(\delta_\lambda, \delta_w)$ with $0 \leq \delta_\lambda \leq \ell_\lambda$ and $0 < \delta_w \leq \ell_w$, as well as

$$2KL_1\delta_w + 2KL_2\delta_\lambda \leq 1 \qquad \text{and} \qquad 2K\varrho + 2KL_3\delta_\lambda + 2KL_4\delta_\lambda^2 \leq \delta_w \ , \tag{21}$$

and for each such pair the following holds. For every $\lambda \in \mathbb{R}$ with $|\lambda - \lambda^*| \leq \delta_\lambda$ there exists a uniquely determined element $w(\lambda) \in \mathcal{X}$ with $\|w(\lambda) - w^*\|_{\mathcal{X}} \leq \delta_w$ such that $\mathcal{F}(\lambda, w(\lambda)) = 0$. In other words, if we define

$$\mathcal{B}^{\mathcal{X}}_{\delta_w} = \left\{ w \in \mathcal{X} \ : \ \left\| w - w^* \right\|_{\mathcal{X}} \leq \delta_w \right\} \quad \text{and} \quad \mathcal{B}^{\mathbb{R}}_{\delta_\lambda} = \left\{ \lambda \in \mathbb{R} \ : \ \left| \lambda - \lambda^* \right| \leq \delta_\lambda \right\} \ ,$$

then all solutions of the nonlinear problem $\mathcal{F}(\lambda, w) = 0$ in the set $\mathcal{B}^{\mathbb{R}}_{\delta_\lambda} \times \mathcal{B}^{\mathcal{X}}_{\delta_w}$ lie on the graph of the function $\lambda \mapsto w(\lambda)$. In addition, the function $\lambda \mapsto w(\lambda)$ is infinitely-many times Fréchet differentiable.

The above theorem is used for all of the results given in the next Section 2.4. The following is a summary of how we approach each of the hypotheses (H1)–(H4).

- The numerical approximation of a potential equilibrium state is found using AUTO [36] in the form of a finite Fourier cosine sum, as described in more detail in Section 3.1.
- The residual bound ϱ in (H1) is computed using the specific norms we use on $\mathcal{Y}$. This is accomplished by evaluating a suitable sum which depends on the Fourier coefficients in this representation using the interval arithmetic package Intlab [37], and makes use of the equivalent Sobolev norms which will be described in Section 3.1 below.
- The inverse norm bound in (H2) is established in Section 4. This estimate is derived in the broad context of (3) and (4) given in Section 1, which contains the triblock copolymer model linearization as a special case. It relies heavily on the framework developed in Sections 3.1, 3.2, and 3.3.
- The Lipschitz estimates given in (H3) and (H4) that are required in the specific case of the triblock copolymer equation are derived in Section 3.4.

The details of these more technical steps of the paper are contained in Sections 3 and 4. First, however, we present some sample results.

2.4. Rigorously verified microstructures

In this section, we illustrate the methods of this paper by rigorously validating equilibrium solutions for the triblock copolymer equation for fixed values of ε, σ, and μ. In particular, Figs. 4, 5, 6, and 7 show numerically computed approximations of solutions. As mentioned before, in these figures, instead of using the parameter ε, we give the results for fixed $\lambda = 1/\varepsilon^2$. From the numerics alone, we cannot guarantee that a qualitatively similar solution exists near the

Table 1
Solution validation information for the one-dimensional solutions depicted in Fig. 4. For all solutions, $\sigma = 6$. Note that the values of K and L_i are computed at higher precision than reported here. They are only given here for illustration of how we establish the two δ values.

Label	μ	λ	N	K	(L_1, L_2, L_3)	δ_α	δ_x
4a	(0.5, 0.5, 0.0)	50	216	19.256	(2.79, 1.45, 0.24)	9.3759e−04	8.8156e−03
4b	(0.5, 0.5, 0.0)	50	242	21.802	(2.71, 1.33, 0.24)	7.7418e−04	8.0867e−03
4c	(0.5, 0.5, 0.1)	50	219	19.595	(2.99, 1.49, 0.26)	8.1679e−04	8.3619e−03
4d	(0.5, 0.4, 0.1)	50	245	21.617	(2.76, 1.40, 0.25)	7.3311e−04	8.0180e−03

computed solution, or if this solution is isolated. However in each case, and using the methods established in the paper, we have rigorously established that for the given parameters there exists a true solution to the triblock copolymer equation within a known fixed distance of the depicted solution, and we specify the distance in each case. Furthermore, we have also validated isolation of the solution. That is, the true solution is unique within a fixed radius ball around the computed solution, which is also explicitly specified in each case.

To implement the verification outlined at the end of the previous section without a parameter search, one must make a tradeoff. Specifically, when applying Theorem 4.1, one must find an integer $N \in \mathbb{N}$ and $\tau > 0$ such that a relation of the form

$$\frac{1}{N^2}\sqrt{A(N)^2 + B^2} \leq \tau < 1 \tag{22}$$

holds, where $A(N)$ and B are constants, and $A(N)$ depends on N. The inverse norm bound is then determined by dividing by $1 - \tau$. This division leads to a tradeoff in the number of basis functions per spatial dimension (N) and the desired sharpness of the norm bound. In practice, we usually target $\tau \approx 0.75$ as this prevents unnecessary inflation of the final bound while remaining computationally feasible. In order to achieve these τ values, we must find an N such that (22) holds. This is difficult to do *a priori* since $A(N)$ depends on the choice of N through a numerical computation. Thus, we make the following simplifying assumptions for an initial estimate of N:

1. $A(N)$ is bounded above as N increases.
2. B dominates $A(N)$ so that $\sqrt{A(N)^2 + B^2} \approx B$.

The latter assumption provides a simple estimation for N that would result in validation:

$$\frac{B}{\tau} \leq N^2.$$

We emphasize this approach simply avoids a computationally intense search for N. Once N is chosen, the value of $A(N)$ can be computed directly as in Theorem 4.1, and (22) can be verified. We take this simplified approach because the specific forms of $A(N)$ and B in Theorem 4.1 satisfy the assumptions, and it provides a more computationally feasible value of N in general. In one dimension, this is not an issue, as the calculation is very quick, a few seconds with Intlab 12 and Matlab 2020b on a Mac mini using an Intel processor with 3.2 GHz and 32 GB memory, under MacOS Monterey. However, for the two-dimensional case, this becomes a larger issue, since the calculation of K for $\lambda = 10$ takes around 20 s, and for $\lambda = 20$ it takes 3–5 min. For λ much larger, the required N results in a full matrix that is too big to keep in memory. We note that these large N values slow our implementation significantly because we use full matrices at every step. However, a vast majority of the entries in these matrices are small in magnitude. For example, in the cases we considered, the observed percentage of matrix entries below 10^{-16} in magnitude is about 97%–98% in one dimension, and in two dimensions, this becomes over 99%. Thus one could assuredly speed up the implementation significantly by using sparse approximations. We leave this to a future effort.

We now describe the selection of example equilibria for which we have rigorously verified stationary solutions. Fig. 4 shows a set of equilibria which have been computed for the μ values $(0.5, 0.5, 0)$ and $(0.5, 0.4, 0.1)$, located in the light blue region for the case of the one-dimensional domain $\Omega = (0, 1)$. In this case, we consider the parameter $\lambda = 50$. For all of the shown equilibrium solutions, we consider the parameter value $\sigma = 6$. Notice that for $\mu_3 = 0$ the triblock copolymer equation reduces to the diblock copolymer model. Therefore, these solutions are respectively equal to and close to cases previously studied in the case of two monomer blocks. In fact, even for $\mu_3 = 0.1$ the triblock copolymer model behaves similarly to the two-component case, and Fig. 2 illustrates this in the left image by showing the bifurcation diagram for the second μ value above in one space dimension. Note that the diagram bears a striking resemblance to the bifurcation diagram for the diblock copolymer equation, see [8,9]. To emphasize that this similarity is based on μ rather than the one spatial dimension, the right image of the figure shows a bifurcation diagram for one space dimension such that $\mu = (0.4, 0.2, 0.4)$, i.e. all three components of μ are far from zero. The diagram is a significant departure from the diblock copolymer case.

We now turn to the case of the two-dimensional square domain $\Omega = (0, 1)^2$. Figs. 5–7 depict equilibria for the triblock copolymer system for the three values of μ in the dark blue region of Fig. 1. Since all three components of μ are significantly nonzero, these cases are quite different from the diblock copolymer case. In order to depict these solutions,

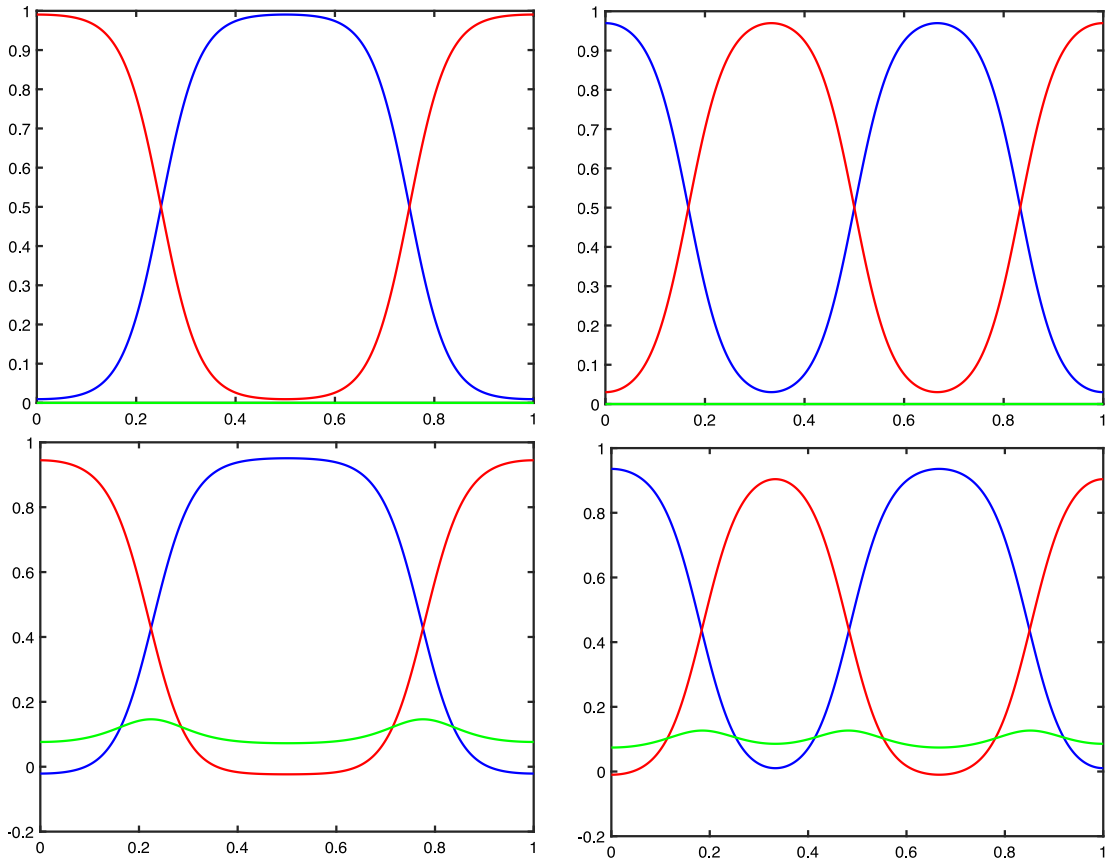

Fig. 4. Sample validated triblock copolymer equilibrium solutions on the one-dimensional domain $\Omega = (0, 1)$. In all figures, we have chosen $\sigma = 6$ and $\lambda = 50$. The top row (left to right: a, b) is for $\mu = (0.5, 0.5, 0.0)$, while the bottom row (c,d) has $\mu = (0.5, 0.4, 0.1)$. In all plots, the solutions u_1, u_2, and u_3 are shown in blue, red, and green, respectively. The validation parameters are listed in Table 1.

Table 2
Solution validation information for the two-dimensional solutions depicted in Figs. 5 and 6. For all solutions, $\sigma = 6$. As with the one-dimensional case, the values of K and L_i are not stated at the full precision that we computed.

Label	μ	λ	N	K	(L_1, L_2, L_3)	δ_α	δ_x
5a	(0.3, 0.2, 0.5)	10	46	968.48	(1.06, 1.54, 0.308)	8.5889e−07	4.9838e−04
5b	(0.3, 0.2, 0.5)	20	86	7898.2	(1.98, 2.01, 0.296)	5.6899e−09	3.1894e−05
5c	(0.3, 0.2, 0.5)	20	98	434.29	(1.95, 1.43, 0.294)	2.3028e−06	5.8787e−04
6a	(0.35, 0.33, 0.32)	10	48	401.17	(0.974, 1.55, 0.277)	6.7908e−06	1.3841e−03
6b	(0.35, 0.33, 0.32)	20	99	572.03	(2.17, 1.85, 0.296)	1.2801e−06	4.1691e−04
6c	(0.35, 0.33, 0.32)	20	97	674.44	(2.04, 1.85, 0.285)	9.9216e−07	3.7167e−04
7a	(0.4, 0.2, 0.4)	10	40	238.08	(0.731, 0.82, 0.248)	3.2873e−05	3.3207e−03
7b	(0.4, 0.2, 0.4)	20	94	361.27	(2.06, 1.80, 0.298)	3.1087e−06	6.6886e−04
7c	(0.4, 0.2, 0.4)	20	80	117.59	(1.84, 1.50, 0.280)	3.4630e−05	2.2780e−03

we have used the pointwise values of the three components (u_1, u_2, u_3), each of which are basically values between 0 and 1, as the RGB values of the resulting image. Therefore, a region which is primarily red corresponds to a region primarily consisting of the first monomer, a green region mostly of the second monomer, and a blue region consisting of the third monomer. In between the almost pure red, green, and blue regions, there are narrow transition layers which usually appear as gray or brown. These contain a mixture of multiple monomers. In fact mixed regions do not only occur in transition layers. For example, in Fig. 7a, there are two large regions of green and purple, where the purple region corresponds to a mixed monomer layer.

Our primary focus in this paper is on establishing the framework necessary for rigorous computation of equilibria, and thus we do not try to give an exhaustive set of connected branches of stationary states. First of all, for each value of μ, there are an enormous number of equilibrium solutions for each λ and σ value, as shown in Fig. 3. In this and all other bifurcation

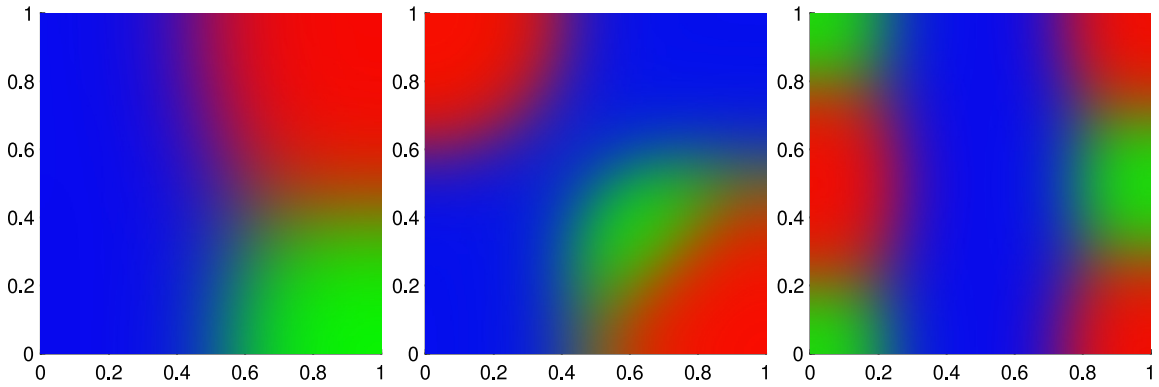

Fig. 5. Sample validated triblock copolymer equilibrium solutions on the two-dimensional domain $\Omega = (0, 1)^2$ and for the parameters $\sigma = 6$, $\mu = (0.3, 0.2, 0.5)$, as well as (left to right) (a) $\lambda = 10$ and (b, c) $\lambda = 20$. The validation parameters are listed in Table 2.

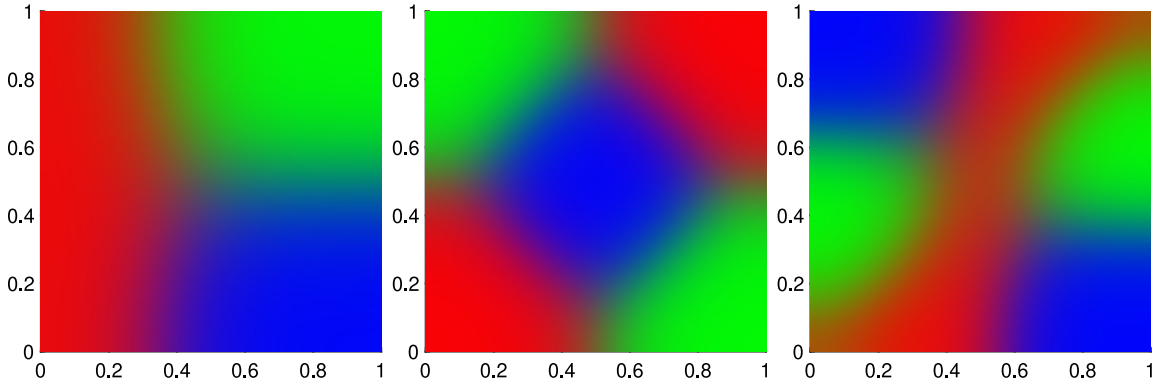

Fig. 6. Sample validated triblock copolymer equilibrium solutions on the two-dimensional domain $\Omega = (0, 1)^2$, where $\sigma = 6$, $\mu = (0.35, 0.33, 0.32)$, and (a) $\lambda = 10$ and (b, c) $\lambda = 20$. The validation parameters are listed in Table 2.

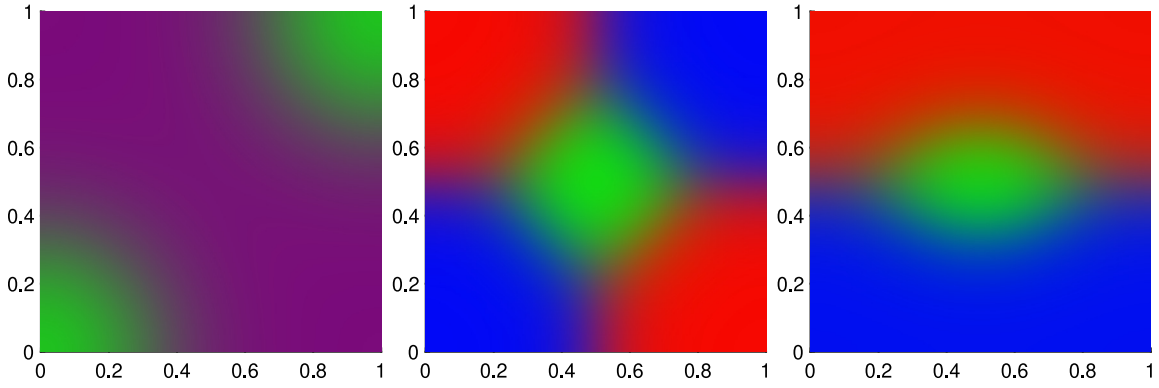

Fig. 7. Sample validated triblock copolymer equilibrium solutions on the two-dimensional domain $\Omega = (0, 1)^2$, where $\sigma = 6$, $\mu = (0.4, 0.2, 0.4)$, and (a) $\lambda = 10$ and (b, c) $\lambda = 20$. The validation parameters are listed in Table 2.

diagrams, we have fixed $\sigma = 6$, but for nearby σ values, the complexity of the figure is consistently large. Therefore it is not realistically tractable to create an exhaustive set of all equilibria. Second, in order to validate branches of solutions, we would need to combine the methods of this paper with the validated pseudo-arclength continuation methods established in [27]. This will also involve new development, since in the context of that paper, they were only applied in a finite-dimensional case. The latter paper creates the first steps, via a more flexible method of estimation. Rather than trying to do everything at once, a systematic study combining these techniques will be the topic of a forthcoming paper.

3. Functional-analytic framework and basic estimates

In this section, we describe the functional-analytic framework for establishing stationary states of the triblock copolymer model using the constructive implicit function theorem from Section 2.3. We will present the underlying spaces and norms, and recall necessary auxiliary results and estimates. The results of the present section reduce the equilibrium verification problem to the derivation of the Fréchet derivative inverse operator norm bound, which is the central result of this paper and will be established in the next section.

More precisely, we begin by discussing the necessary function spaces in Section 3.1, which form the foundation for our spectral approach based on Fourier cosine series. The following Section 3.2 recalls a number of rigorous Sobolev embedding results that originated in [38], and results which allow us to replace the standard Sobolev norms with more computationally appropriate ones. Section 3.3 is devoted to the required finite-dimensional approximation spaces and associated projection operators, which are used in our computer-assisted proofs. Finally, in Section 3.4 we derive the necessary Lipschitz estimates for the Fréchet derivatives of the underlying nonlinear operator. Once that is accomplished, the only missing piece of the puzzle is then the norm bound for the inverse, and this is left for Section 4 of the paper.

3.1. Fourier cosine series expansions and Sobolev spaces

As mentioned in the last section, the functional-analytic backdrop for our equilibrium validation are the spaces $\bar{H}^2_n(\Omega)$ and $\bar{H}^{-2}_n(\Omega)$ introduced in (16). These spaces are considered on the unit cube $\Omega = (0,1)^d$ in dimension $d = 1, 2, 3$, and they incorporate both the zero mass constraint and the homogeneous Neumann boundary conditions. Important for our spectral approach is the fact that Fourier cosine series forms a complete orthogonal set in both spaces. To describe this in more detail, define the constants $c_0 = 1$ and $c_\ell = \sqrt{2}$ for $\ell \in \mathbb{N}$. Furthermore, we will make use of multi-indices $k \in \mathbb{N}_0^d$ of the form $k = (k_1, \dots, k_d)$ and let

$$c_k = c_{k_1} \cdot \ldots \cdot c_{k_d} \ .$$

If one then defines

$$\varphi_k(x) = c_k \prod_{i=1}^{d} \cos(k_i \pi x_i) \qquad \text{for all} \qquad x = (x_1, \dots, x_d) \in \Omega \ , \tag{23}$$

then the family $\{\varphi_k\}_{k\in\mathbb{N}_0^d}$ is a complete orthonormal basis for the space $L^2(\Omega)$. Thus, any measurable and square-integrable function $u : \Omega \to \mathbb{R}$ can be written in terms of its Fourier cosine series

$$u(x) = \sum_{k\in\mathbb{N}_0^d} \alpha_k \varphi_k(x) \ , \tag{24}$$

where the real numbers $\alpha_k \in \mathbb{R}$ are the Fourier cosine coefficients of u, and we have

$$\|u\|_{L^2} = \left(\sum_{k\in\mathbb{N}_0^d} \alpha_k^2 \right)^{1/2} \ ,$$

where $\|\cdot\|_{L^2}$ denotes the standard $L^2(\Omega)$-norm on the above domain Ω. To simplify notation, we further introduce the abbreviations

$$|k| = \left(k_1^2 + \cdots + k_d^2\right)^{1/2} \qquad \text{and} \qquad |k|_\infty = \max(k_1, \dots, k_d)$$

to distinguish between the Euclidean and maximum norms of multi-indices.

Recall that each function φ_k is an eigenfunction of the negative Laplacian subject to homogeneous Neumann boundary conditions. The corresponding eigenvalue is given by κ_k, and is defined via the equations

$$-\Delta\varphi_k = \kappa_k \varphi_k \qquad \text{with} \qquad \kappa_k = \pi^2 \left(k_1^2 + k_2^2 + \cdots + k_d^2\right) = \pi^2 |k|^2. \tag{25}$$

Notice also that every function φ_k satisfies the identity $\partial(\Delta\varphi_k)/\partial\nu = -\kappa_k \partial\varphi_k/\partial\nu = 0$, i.e., any finite Fourier cosine series as above automatically satisfies both imposed boundary conditions of the triblock copolymer equation (1).

It will be useful to think of our basic function spaces in terms of the Fourier cosine series representation in (24). Thus, for $\ell \in \mathbb{N}$ we consider the space

$$\mathcal{H}^\ell = \left\{ u = \sum_{k\in\mathbb{N}_0^d} \alpha_k \varphi_k : \|u\|_{\mathcal{H}^\ell} < \infty \right\} \qquad \text{with} \qquad \|u\|^2_{\mathcal{H}^\ell} = \sum_{k\in\mathbb{N}_0^d} \left(1 + \kappa_k^\ell\right) \alpha_k^2 \ ,$$

where the latter identity is equivalent to

$$\|u\|^2_{\mathcal{H}^\ell} = \|u\|^2_{L^2} + \left\|(-\Delta)^{\ell/2} u\right\|^2_{L^2} \ ,$$

and the fractional Laplacian for odd ℓ is defined using the spectral definition. One can show that the above spaces are subspaces of the standard Sobolev spaces $H^k(\Omega) = W^{k,2}(\Omega)$, which were discussed in [39]. In addition, notice that for sufficiently large ℓ, their definition automatically incorporates the boundary conditions of (1). For example, we have $\mathcal{H}^0 = L^2(\Omega)$ and $\mathcal{H}^1 = H^1(\Omega)$, as well as

$$\mathcal{H}^2 = \left\{ u \in H^2(\Omega) : \frac{\partial u}{\partial \nu} = 0 \right\} \quad \text{and} \quad \mathcal{H}^4 = \left\{ u \in H^4(\Omega) : \frac{\partial u}{\partial \nu} = \frac{\partial \Delta u}{\partial \nu} = 0 \right\} ,$$

where the boundary conditions in the last two equations are considered in the sense of the trace operator. See [16] for more details on these identities.

While the spaces $\mathcal{H}^\ell$ incorporate the boundary conditions of (1), in the last section we reformulated the triblock copolymer model so that both solution components satisfy the integral constraint $\int_\Omega u \, dx = 0$, since the case of nonzero mass average has been absorbed into the placement of the parameters μ_1 and μ_2. This mass constraint can be incorporated by considering suitable subspaces of $\mathcal{H}^\ell$. To this end, consider an arbitrary integer $\ell \in \mathbb{Z}$ and define the space

$$\overline{\mathcal{H}}^\ell = \left\{ u = \sum_{k \in \mathbb{N}_0^d,\ |k|>0} \alpha_k \varphi_k \ : \ \|u\|_{\overline{\mathcal{H}}^\ell} < \infty \right\} \quad \text{with} \quad \|u\|_{\overline{\mathcal{H}}^\ell}^2 = \sum_{k \in \mathbb{N}_0^d,\ |k|>0} \kappa_k^\ell \alpha_k^2 . \tag{26}$$

We would like to point out that in these reduced spaces, we use a simpler norm than the one used in $\mathcal{H}^\ell$. For $\ell = 0$ this definition reduces to the subspace of $L^2(\Omega)$ of all functions with average zero, equipped with its standard norm, while for $\ell > 0$ we have $\overline{\mathcal{H}}^\ell \subset \mathcal{H}^\ell$ and the new norm is equivalent to the original norm on $\mathcal{H}^\ell$. Moreover, note that in the case of a negative integer $\ell < 0$ the series in (24) is interpreted formally, i.e., the element $u \in \overline{\mathcal{H}}^\ell$ is identified with the sequence of its Fourier cosine coefficients. One can verify that in this case u acts as a bounded linear functional on $\overline{\mathcal{H}}^{-\ell}$. In fact, for all $\ell < 0$ the space $\overline{\mathcal{H}}^\ell$ can be considered as a subspace of the negative exponent Sobolev space $H^\ell(\Omega) = W^{\ell,2}(\Omega)$, see again [39]. Finally, for every $\ell \in \mathbb{Z}$ the space $\overline{\mathcal{H}}^\ell$ is a Hilbert space with inner product

$$(u, v)_{\overline{\mathcal{H}}^\ell} = \sum_{k \in \mathbb{N}_0^d,\ |k|>0} \kappa_k^\ell \alpha_k \beta_k , \tag{27}$$

where

$$u = \sum_{k \in \mathbb{N}_0^d,\ |k|>0} \alpha_k \varphi_k \in \overline{\mathcal{H}}^\ell \qquad \text{and} \qquad v = \sum_{k \in \mathbb{N}_0^d,\ |k|>0} \beta_k \varphi_k \in \overline{\mathcal{H}}^\ell .$$

Being separable Hilbert spaces, the spaces $\overline{\mathcal{H}}^\ell$ do have complete orthonormal sets. The most important one for us is the one given via rescalings of the functions φ_k, which is identified in the following lemma. Its straightforward proof is left to the reader.

Lemma 3.1 (*Complete Orthonormal Set in $\overline{\mathcal{H}}^\ell$*)**.** *For every $\ell \in \mathbb{Z}$ a complete orthonormal set in the Hilbert space $\overline{\mathcal{H}}^\ell$ is given by the family* $\left\{ \kappa_k^{-\ell/2} \varphi_k(x) \right\}_{k \in \mathbb{N}_0^d,\ |k|>0}$.

The above spaces are the foundation for our functional-analytic setting. Notice that using these spaces, we can equivalently reformulate the equilibrium system (15), as written in (17) and (19), using the space notation in (18). It is clear from our above discussion that we have

$$\mathcal{X} = \overline{\mathcal{H}}^2 \times \overline{\mathcal{H}}^2 \qquad \text{and} \qquad \mathcal{Y} = \overline{\mathcal{H}}^{-2} \times \overline{\mathcal{H}}^{-2} , \tag{28}$$

where on these product spaces we use the norms

$$\|(w_1, w_2)\|_{\mathcal{X}}^2 = \|w_1\|_{\overline{\mathcal{H}}^2}^2 + \|w_2\|_{\overline{\mathcal{H}}^2}^2 \quad \text{and} \quad \|(w_1, w_2)\|_{\mathcal{Y}}^2 = \|w_1\|_{\overline{\mathcal{H}}^{-2}}^2 + \|w_2\|_{\overline{\mathcal{H}}^{-2}}^2 . \tag{29}$$

Notice that the nonlinear problem $\mathcal{F}(\lambda, w) = 0$ is now formulated weakly, and in particular, the second boundary condition $\partial(\Delta w_i)/\partial \nu = 0$ for $i = 1, 2$ is no longer explicitly stated in this weak formulation. Note, however, that the first boundary conditions $\partial w_i/\partial \nu = 0$ have been incorporated into the space $\mathcal{X}$. Furthermore, the fact that the functions f_1 and f_2 in (19) are both of class C^2 is sufficient to guarantee that the function $\mathcal{F} : \mathbb{R} \times \mathcal{X} \to \mathcal{Y}$ is well-defined and Fréchet differentiable, since we only consider domains up to dimension three.

3.2. Constructive Sobolev embeddings and norm bounds

We now turn our attention to a number of auxiliary results which relate the norms of the spaces from the last subsections to each other, as well as to other norms. Needless to say, all of these results need to be explicit with concrete bounds, since they will be used in a constructive computer-assisted proof setting. We begin by recalling two classical results concerning Sobolev spaces — namely the Sobolev embedding theorem and the Banach algebra estimate in the

Table 3
The table contains the explicit values for the constants introduced in Lemma 3.2, depending on the domain dimension d. They were derived using rigorous computational techniques in [16,38].

Dimension d	1	2	3
Sobolev embedding constant C_m	1.010947	1.030255	1.081202
Sobolev embedding constant $\overline{C}_m$	0.149072	0.248740	0.411972
Banach algebra constant C_b	1.471443	1.488231	1.554916

Sobolev space of order two. These results relate the norms on the function spaces $\overline{\mathcal{H}}^2$ and $\mathcal{H}^2$ to each other, as well as to the classical infinity norm. As a side result, we obtain that all functions in $\mathcal{H}^2$ are in fact continuous functions on $\overline{\Omega}$, and that $\mathcal{H}^2$ is closed under multiplication. These results are essential for the results of the next section.

Lemma 3.2 (*Sobolev Embeddings and Banach Algebra Estimates*)**.** *Consider the Hilbert spaces $\mathcal{H}^2$ and $\overline{\mathcal{H}}^2$ from the last subsection, which are defined over the unit cube $\Omega = (0,1)^d$ for dimensions $d = 1, 2, 3$. Then the following statements hold:*

(a) **Sobolev embedding:** *For all $u \in \mathcal{H}^2$ and arbitrary $\bar{u} \in \overline{\mathcal{H}}^2$ the estimates*

$$\|u\|_\infty \leq C_m \|u\|_{\mathcal{H}^2} \qquad \text{and} \qquad \|\bar{u}\|_\infty \leq \overline{C}_m \|\bar{u}\|_{\overline{\mathcal{H}}^2}$$

are satisfied, where the constants C_m and $\overline{C}_m$ can be found in Table 3, and $\|\cdot\|_\infty$ denotes the supremum norm in $L^\infty(\Omega)$. In particular, these estimates show that every function in $\mathcal{H}^2$ is almost everywhere equal to a continuous function on $\overline{\Omega}$.

(b) **Banach algebra estimate:** *For all $u, v \in \mathcal{H}^2$ we have*

$$\|uv\|_{\mathcal{H}^2} \leq C_b \|u\|_{\mathcal{H}^2} \|v\|_{\mathcal{H}^2} ,$$

where the constant C_b can be found in Table 3. In other words, the Sobolev space $\mathcal{H}^2$ is closed under multiplication.

(c) **Explicit norm equivalence:** *For all $\bar{u} \in \overline{\mathcal{H}}^2$ we have*

$$\|\bar{u}\|_{\overline{\mathcal{H}}^2} \leq \|\bar{u}\|_{\mathcal{H}^2} \leq C_e \|\bar{u}\|_{\overline{\mathcal{H}}^2} \qquad \text{with} \qquad C_e = \frac{\sqrt{1+\pi^4}}{\pi^2} .$$

The proofs for the first inequality in *(a)* and the inequality in *(b)* can be found in [38]. The remaining statements were established in [16]. Many of these estimates were themselves obtained via computer-assisted proofs, see again the mentioned references.

Our next and final result of this subsection discusses the relation between the spaces $\overline{\mathcal{H}}^\ell$ for varying values of the differentiation order ℓ, i.e., we discuss the so-called scale of these spaces. More precisely, it shows that, on the one hand, due to our norm choices the Laplacian acts as an isometry between spaces of appropriate differentiation orders. On the other hand, it provides explicit embedding constants from spaces with larger differentiation order to ones with smaller order. The proof of the following lemma can be found in [16].

Lemma 3.3 (*Sobolev Scale Properties*)**.** *Consider the Hilbert spaces $\mathcal{H}^\ell$ for $\ell \in \mathbb{Z}$ from the last subsection, which are defined over the unit cube $\Omega = (0,1)^d$ for $d = 1, 2, 3$. Then the following statements hold:*

(a) **Laplacian isometry:** *For every integer $\ell \in \mathbb{Z}$ the Laplacian operator Δ is an isometry from $\overline{\mathcal{H}}^\ell$ to $\overline{\mathcal{H}}^{\ell-2}$, i.e., for all $u \in \overline{\mathcal{H}}^\ell$ the identities*

$$\|\Delta^{-1} u\|_{\overline{\mathcal{H}}^{\ell+2}} = \|u\|_{\overline{\mathcal{H}}^\ell} = \|\Delta u\|_{\overline{\mathcal{H}}^{\ell-2}}$$

are satisfied.

(b) **Scale embeddings:** *For all $u \in \overline{\mathcal{H}}^m$ and all $\ell \leq m$ we have the estimate*

$$\|u\|_{\overline{\mathcal{H}}^\ell} \leq \frac{1}{\pi^{m-\ell}} \|u\|_{\overline{\mathcal{H}}^m} .$$

Furthermore, note that in the special case $\ell = 0 \leq m$ we have $\|u\|_{\overline{\mathcal{H}}^0} = \|u\|_{L^2}$.

3.3. Spectral projection operators

We now turn our attention to the finite-dimensional approximation spaces that will be used in our computer-assisted existence proofs for equilibrium solutions of (1). These turn out to simply be generated by truncated cosine series, and this is briefly recalled in the present subsection via suitable projection operators.

For this, let $N \in \mathbb{N}$ denote a positive integer, and consider $u \in \mathcal{H}^\ell$ for $\ell \in \mathbb{N}_0$, or alternatively $u \in \overline{\mathcal{H}}^\ell$ for $\ell \in \mathbb{Z}$, of the form $u = \sum_{k\in\mathbb{N}_0^d} \alpha_k \varphi_k$, where in the latter case $\alpha_0 = 0$. Then as in [16] we define the projection

$$P_N u = \sum_{k\in\mathbb{N}_0^d,\ |k|_\infty < N} \alpha_k \varphi_k \ . \tag{30}$$

In this definition we use the ∞-norm of the multi-index k, since this simplifies the implementation aspects of our method. The so-defined operator P_N is a bounded linear operator on $\mathcal{H}^\ell$ with induced operator norm equal to 1, and it leaves the space $\overline{\mathcal{H}}^\ell$ invariant if $\ell \in \mathbb{Z}$. Moreover, one can easily show that for any $N \in \mathbb{N}$ we have

$$\dim P_N \mathcal{H}^\ell = N^d \qquad \text{and} \qquad \dim P_N \overline{\mathcal{H}}^\ell = N^d - 1 \ . \tag{31}$$

Notice also that for all $\ell \in \mathbb{N}_0$ the identity $(I - P_1)\mathcal{H}^\ell = \overline{\mathcal{H}}^\ell$ holds. Since this is an especially useful operator, we introduce the abbreviation

$$\overline{P} = I - P_1 \ . \tag{32}$$

It was shown in [16] that this operator $\overline{P}$ satisfies the identity

$$\big(\overline{P}u, v\big)_{L^2} \ = \ (u, v)_{L^2} \qquad \text{for all} \qquad u \in \mathcal{H}^0 \quad \text{and} \quad v \in \overline{\mathcal{H}}^0. \tag{33}$$

To close this subsection, we present a norm bound for the infinite Fourier cosine series part that is discarded by the projection P_N in terms of a higher-regularity norm. More precisely, we have the following result, whose proof can again be found in [16].

Lemma 3.4 (*Projection Tail Estimates*). *Consider two integers $\ell \le m$ and let $u \in \overline{\mathcal{H}}^m$ be arbitrary. Then the projection tail $(I - P_N)u$ satisfies the estimate*

$$\|(I - P_N)u\|_{\overline{\mathcal{H}}^\ell} \ \le \ \frac{1}{\pi^{m-\ell} N^{m-\ell}} \, \|(I - P_N)u\|_{\overline{\mathcal{H}}^m} \ \le \ \frac{1}{\pi^{m-\ell} N^{m-\ell}} \, \|u\|_{\overline{\mathcal{H}}^m} \ .$$

3.4. Lipschitz bounds for the Fréchet derivatives

To close this section, we now turn our attention to the Lipschitz bounds which are required in hypotheses (H3) and (H4) of the constructive implicit function theorem. The basic idea for their derivation is the same as in [16], and it makes use of the explicit form of the Fréchet derivatives of $\mathcal{F}$ with respect to w and λ, combined with a suitable version of the mean value theorem and our estimates from Section 3.2. In this way, we obtain the following result.

Lemma 3.5 (*Lipschitz Bounds for the Fréchet Derivatives of $\mathcal{F}$*). *Consider the nonlinear triblock copolymer operator $\mathcal{F} : \mathbb{R} \times \mathcal{X} \to \mathcal{Y}$ defined in (19), between the spaces introduced in (18). Then both Hypotheses (H3) and (H4) are satisfied with the explicit constants*

$$\begin{aligned} L_1 \ &= \ \frac{2^{3/2}\overline{C}_m(|\lambda^*| + \ell_\lambda) f^{(2)}_{\max}}{\pi^2} \ , & L_2 \ &= \ \frac{f^{(1)}_*}{\pi^2} + \frac{\sigma}{\pi^4} \ , \\ L_3 \ &= \ \frac{2 f^{(1)}_{\max}}{\pi^2} + \frac{\sigma}{\pi^4} \ , \quad \textit{and} & L_4 \ &= \ 0 \ , \end{aligned} \tag{34}$$

where the values $f^{(2)}_{\max}$, $f^{(1)}_{\max}$, and $f^{(1)}_*$ are defined in (35) and (36) below, and the value of $\overline{C}_m$ can be found in Table 3.

Proof. In the following, we recall that the μ_i are constants representing the total mass of the ith monomer and that w_i are defined as $u_i - \mu_i$ (i.e., the zero-mass component of u_i) to reformulate (8) as (15). For brevity, we use the abbreviation $\mu + w = (\mu_1 + w_1, \mu_2 + w_2)$, and we denote the Jacobian matrix of $f = (f_1, f_2)$ at a point $z \in \mathbb{R}^2$ by $Df(z) = (\nabla f_1(z), \nabla f_2(z))^t$. Recall that the Fréchet derivative of the nonlinear operator $\mathcal{F}$ is then explicitly given by

$$\begin{aligned} D_w \mathcal{F}(\lambda, w)[\tilde{w}] \ &= \ -\Delta(\Delta\tilde{w} + \lambda Df(\mu + w)\tilde{w}) - \lambda\sigma\tilde{w} \\ &= \ \begin{pmatrix} -\Delta\left(\Delta\tilde{w}_1 + \lambda\nabla f_1(\mu + w)\cdot\tilde{w}\right) - \lambda\sigma\tilde{w}_1 \ , \\ -\Delta\left(\Delta\tilde{w}_2 + \lambda\nabla f_2(\mu + w)\cdot\tilde{w}\right) - \lambda\sigma\tilde{w}_2 \end{pmatrix} \ . \end{aligned}$$

In the following proof, we will make frequent use of the results from the last three subsections. For a pair of functions $w = (w_1, w_2)$ in either $\mathcal{X}$ or $\mathcal{Y}$ defined in (28), we use the respective norms given in (29). In addition, and parallel to these definitions, we define the norms $\|\cdot\|_{\mathcal{Z}}$ by $\|w\|^2_{\mathcal{Z}} = \|w_1\|^2_{\mathcal{H}^0} + \|w_2\|^2_{\mathcal{H}^0}$, and the norm $\|\cdot\|_{\mathcal{I}}$ by $\|w\|^2_{\mathcal{I}} = \|w_1\|^2_\infty + \|w_2\|^2_\infty$. Finally, if w^* denotes the solution approximation from the constructive implicit function theorem, then we define the set $R = \{z \in \mathbb{R}^2 \ : \ \|z\| \le \|w^*\|_{\mathcal{I}} + \overline{C}_m \ell_w\}$, the constants

$$f^{(1)}_{\max} \ = \ \max_{\substack{i,j=1,2 \\ z\in R}} \left|\frac{\partial f_i}{\partial z_j}(z + \mu)\right| \quad \text{and} \quad f^{(2)}_{\max} = \max_{\substack{i,j,k=1,2 \\ z\in R}} \left|\frac{\partial^2 f_i}{\partial z_k \partial z_j}(z + \mu)\right| \ , \tag{35}$$

as well as finally the constant

$$f_*^{(1)} = \max_{i,j=1,2} \left\| \frac{\partial f_i}{\partial z_j}(w^* + \mu) \right\|_\infty . \tag{36}$$

Consider now any two scalar norms $\|\cdot\|_{s_1}, \|\cdot\|_{s_2}$ and two vector norms $\|\cdot\|_{S_1}, \|\cdot\|_{S_2}$ which are related by the identity $\|(w_1, w_2)\|_{S_i}^2 = \|w_1\|_{s_i}^2 + \|w_2\|_{s_i}^2$. Assume further that for every scalar function u such that the s_i norms are well-defined one has the estimate $\|u\|_{s_1} \leq C\|u\|_{s_2}$ for some constant $C > 0$. Then the corresponding estimate is satisfied with unchanged C also in the vector-valued case, i.e., one has $\|w\|_{S_1} \leq C\|w\|_{S_2}$. Therefore, we can use the norm bounds relating the spaces $\overline{\mathcal{H}}^{-2}$, $\overline{\mathcal{H}}^{2}$, $\overline{\mathcal{H}}^{0}$, and $C(\overline{\Omega})$ given in Lemmas 3.2 and 3.3 to establish norm bounds relating the spaces $\mathcal{X}$, $\mathcal{Y}$, $\mathcal{Z} = \mathcal{H}^0 \times \mathcal{H}^0$, and $\mathcal{I} = C(\overline{\Omega}) \times C(\overline{\Omega})$, respectively. In particular, Lemmas 3.2*(a)* and 3.3*(a),(b)* imply the four statements

$$\|w\|_{\mathcal{I}} \leq \overline{C}_m \|w\|_{\mathcal{X}} \quad \text{and} \quad \|\Delta w\|_{\mathcal{Y}} = \|w\|_{\mathcal{Z}} , \quad \text{as well as} \tag{37}$$

$$\|w\|_{\mathcal{Z}} \leq \pi^{-2} \|w\|_{\mathcal{X}} \quad \text{and} \quad \|w\|_{\mathcal{Y}} \leq \pi^{-4} \|w\|_{\mathcal{X}} . \tag{38}$$

In preparation for the verification of the actual Lipschitz estimate of the theorem, we consider a smooth function $h : \mathbb{R}^m \to \mathbb{R}^m$, and let $Dh(z)$ denote the Jacobian matrix of h at $z \in \mathbb{R}^m$. Moreover, consider two points $z, \hat{z} \in \mathbb{R}^m$, let $y \in \mathbb{R}^m$, and let $\mathcal{D}$ denote the line segment between z and $\hat{z}$. Then the mean value theorem applied to the kth component of h yields

$$\left| h_k(z) - h_k(\hat{z}) \right| \leq \max_{c \in \mathcal{D}} \|\nabla h_k(c)\|_2 \, \|z - \hat{z}\|_2 \leq \sqrt{m} \max_{\substack{j=1,\dots,m \\ c \in \mathcal{D}}} \left| \frac{\partial h_k}{\partial z_j}(c) \right| \|z - \hat{z}\|_2 ,$$

and thus

$$\|h(z) - h(\hat{z})\|_2 \leq m \max_{\substack{j,k=1,\dots,m \\ c \in \mathcal{D}}} \left| \frac{\partial h_k}{\partial z_j}(c) \right| \|z - \hat{z}\|_2 . \tag{39}$$

In addition, we have

$$\left\| (Dh(z) - Dh(\hat{z}))y \right\|_2^2 = \sum_{k=1}^{m} \left((\nabla h_k(z) - \nabla h_k(\hat{z}))y \right)^2 .$$

Notice that

$$\left| (\nabla h_k(z) - \nabla h_k(\hat{z}))y \right| \leq \left\| \nabla h_k(z) - \nabla h_k(\hat{z}) \right\|_2 \|y\|_2 ,$$

as well as

$$\left| \frac{\partial h_k}{\partial z_j}(z) - \frac{\partial h_k}{\partial z_j}(\hat{z}) \right| \leq \sqrt{m} \max_{\substack{i=1,\dots,m \\ c \in \mathcal{D}}} \left| \frac{\partial^2 h_k}{\partial z_i \partial z_j}(c) \right| \|z - \hat{z}\|_2 ,$$

and therefore

$$\|\nabla h_k(z) - \nabla h_k(\hat{z})\|_2 \leq m \max_{\substack{i,j=1,\dots,m \\ c \in \mathcal{D}}} \left| \frac{\partial^2 h_k}{\partial z_i \partial z_j}(c) \right| \|z - \hat{z}\|_2 .$$

This finally implies

$$\begin{aligned} \left\| (Dh(z) - Dh(\hat{z}))y \right\|_2 &\leq m \left(\sum_{k=1}^{m} \max_{\substack{i,j=1,\dots,m \\ c \in \mathcal{D}}} \left| \frac{\partial^2 h_k}{\partial z_i \partial z_j}(c) \right|^2 \right)^{1/2} \|z - \hat{z}\|_2 \|y\|_2 \\ &\leq m^{3/2} \max_{\substack{i,j,k=1,\dots,m \\ c \in \mathcal{D}}} \left| \frac{\partial^2 h_k}{\partial z_i \partial z_j}(c) \right| \|z - \hat{z}\|_2 \|y\|_2 . \end{aligned} \tag{40}$$

Note that the above computations are similar in spirit to the ones found in [27].

After these preparations, we finally turn our attention to the Lipschitz estimates of the theorem. From the explicit form of the Fréchet derivative $D_w \mathcal{F}$ one obtains

$$\begin{aligned} &\left\| D_w \mathcal{F}(\lambda, w)\tilde{w} - D_w \mathcal{F}(\lambda^*, w^*)\tilde{w} \right\|_{\mathcal{Y}} \\ &\quad = \left\| -\Delta \left(\lambda Df(\mu + w)\tilde{w} - \lambda^* Df(\mu + w^*)\tilde{w} \right) - \left(\lambda - \lambda^* \right) \sigma \tilde{w} \right\|_{\mathcal{Y}} \\ &\quad \leq \left| \lambda - \lambda^* \right| \left(\|\Delta \left(Df(\mu + w)\tilde{w} \right)\|_{\mathcal{Y}} + \sigma \|\tilde{w}\|_{\mathcal{Y}} \right) \\ &\qquad + \left| \lambda^* \right| \|\Delta \left(\left(Df(\mu + w) - Df(\mu + w^*) \right) \tilde{w} \right)\|_{\mathcal{Y}} . \end{aligned}$$

Then the second statement in (37), together with the observation that the components of $Df(\mu+w)\tilde{w}$ do not necessarily have total mass 0, yields

$$\begin{aligned}\|\Delta\,(Df(\mu+w)\tilde{w})\|_{\mathcal{Y}} &\le \|Df(\mu+w)\tilde{w}\|_{\mathcal{Z}} \\ &\le \left\|(Df(\mu+w)-Df(\mu+w^*))\tilde{w}\right\|_{\mathcal{Z}} + \left\|Df(\mu+w^*)\tilde{w}\right\|_{\mathcal{Z}}\ .\end{aligned}$$

Let $\xi(x)\in\mathbb{R}^2$ be a point on the line segment between the vectors $w(x)$ and $w^*(x)$. Then one can bound $\|\xi\|_{\mathcal{I}}$ via

$$\|\xi\|_{\mathcal{I}} \ \le\ \|w^*\|_{\mathcal{I}} + \|w-w^*\|_{\mathcal{I}} \ \le\ \|w^*\|_{\mathcal{I}} + \overline{C}_m\|w-w^*\|_{\mathcal{X}} \ \le\ \|w^*\|_{\mathcal{I}} + \overline{C}_m\ell_w\ .$$

We would like to point out that this last inequality implies that for the region R used in the definitions of both $f^{(1)}_{\max}$ and $f^{(2)}_{\max}$ one therefore obtains $\xi(x)\in R$. Together with (37), (38), and (40) this furnishes

$$\begin{aligned}\left\|(Df(w+\mu)-Df(w^*+\mu))\tilde{w}\right\|_{\mathcal{Z}} &\le 2^{3/2}f^{(2)}_{\max}\|w-w^*\|_{\mathcal{I}}\|\tilde{w}\|_{\mathcal{Z}} \\ &\le \frac{2^{3/2}\overline{C}_m f^{(2)}_{\max}}{\pi^2}\,\|w-w^*\|_{\mathcal{X}}\|\tilde{w}\|_{\mathcal{X}}\ .\end{aligned}$$

Additionally, we have

$$\left\|Df(\mu+w^*)\tilde{w}\right\|_{\mathcal{Z}} \ \le\ \max_{\substack{i,j=1,2\\ x\in\Omega}}\left\|\frac{\partial f_i}{\partial z_j}(\mu+w^*(x))\right\|_{\infty}\|\tilde{w}\|_{\mathcal{Z}} \ \le\ f^{(1)}_*\|\tilde{w}\|_{\mathcal{Z}} \ \le\ \frac{f^{(1)}_*}{\pi^2}\,\|\tilde{w}\|_{\mathcal{X}}\ .$$

Combining the above statements along with the statements in (38), we further see that

$$\begin{aligned}&\|D_w\mathcal{F}(\lambda,w)\tilde{w}-D_w\mathcal{F}(\lambda^*,w^*)\tilde{w}\|_{\mathcal{Y}} \\ &\quad\le\ \left(\frac{f^{(1)}_*}{\pi^2}+\frac{\sigma}{\pi^4}\right)|\lambda-\lambda^*|\,\|\tilde{w}\|_{\mathcal{X}} \ +\ \left(\frac{2^{3/2}\overline{C}_m(|\lambda^*|+\ell_\lambda)f^{(2)}_{\max}}{\pi^2}\right)\|w-w^*\|_{\mathcal{X}}\,\|\tilde{w}\|_{\mathcal{X}}\ ,\end{aligned}$$

which immediately establishes the values of L_1 and L_2 in hypothesis (H3). As for the condition in (H4), we recall that

$$D_\lambda\mathcal{F}(\lambda,w) \ =\ -\Delta(f(\mu+w))-\sigma w\ ,$$

and using the estimate in (39) one further obtains

$$\begin{aligned}\|D_\lambda\mathcal{F}(\lambda,w)-D_\lambda\mathcal{F}(\lambda^*,w^*)\|_{\mathcal{Y}} &\le \left\|\Delta(f(\mu+w)-f(\mu+w^*))\right\|_{\mathcal{Y}}+\sigma\|w-w^*\|_{\mathcal{Y}} \\ &\le \left\|f(\mu+w)-f(\mu+w^*)\right\|_{\mathcal{Z}}+\frac{\sigma}{\pi^4}\|w-w^*\|_{\mathcal{X}} \\ &\le \left(\frac{2f^{(1)}_{\max}}{\pi^2}+\frac{\sigma}{\pi^4}\right)\|w-w^*\|_{\mathcal{X}}.\end{aligned}$$

This finally establishes the values for L_3 and L_4, and completes the proof of Lemma 3.5. □

4. Inverse norm bound for fourth-order elliptic operators

This section is devoted to establishing an inverse bound for the operator L defined in (3) and (4). This bound can be used in various applications to obtain hypothesis (H2), which is required for Theorem 2.2, the constructive implicit function theorem. More precisely, our goal in the following is to derive a constant K such that

$$\left\|L^{-1}\right\|_{\mathcal{L}(\mathbf{Y},\mathbf{X})}\le K\ ,$$

i.e., we need to find a bound on the operator norm of the inverse of the linear operator L. We divide the derivation of this estimate into four parts. In Section 4.1 we give an outline of our approach, introduce necessary definitions and auxiliary results, and present the main result of this section. This result will be verified in the following three sections. First, we discuss the finite-dimensional projection of L in Section 4.2. Using this finite-dimensional operator, we then construct an approximate inverse in Section 4.3, before everything is assembled to provide the desired estimate in the final Section 4.4. In contrast to the discussion of Section 2.3, we use a formulation where the main space $\mathbf{X}$ is a product space of m scalar constraints and n subspaces of $\overline{\mathcal{H}}^2$, namely $\mathbf{X}=\mathbb{R}^m\times\prod_{i=1}^n U_i$. As mentioned in the introduction, this is in preparation of future applications of this theory, which go well beyond the triblock copolymer model.

4.1. General outline and auxiliary results

For every $i=1,\dots,n$, let $U_i\subset\overline{\mathcal{H}}^2$ be a closed subspace and let $\mathcal{J}_i$ denote an infinite index set consisting of multi-indices such that $\{\varphi_k : k\in\mathcal{J}_i\}$ forms a complete orthogonal set of U_i, where the considered basis functions φ_k were introduced in (23). We emphasize that U_i is not necessarily all of $\overline{\mathcal{H}}^2$, but it is critical to have a complete orthogonal

set for each U_i which consists of a subset of the basis functions in (23). We may now form a complete orthogonal set for $\mathbf{X} = \mathbb{R}^m \times \prod_{i=1}^n U_i$ by using the standard basis $\{e_j\}_{j=1}^m$ for $\mathbb{R}^m$ and $\{\varphi_k : k \in \mathcal{J}_i\}$ for every $i = 1, \ldots, n$ as

$$\mathcal{B}_{\mathcal{J}} = \left\{ e_j \times 0_{\left(\overline{\mathcal{H}}^2\right)^n} \right\}_{j=1\ldots m} \bigcup \left\{ 0_{\mathbb{R}^m \times \left(\overline{\mathcal{H}}^2\right)^{i-1}} \times \varphi_k \times 0_{\left(\overline{\mathcal{H}}^2\right)^{n-i}} \right\}_{i=1\ldots n,\, k \in \mathcal{J}_i} \tag{41}$$

where $\mathcal{J} = \{\mathcal{J}_1, \mathcal{J}_2, \ldots, \mathcal{J}_n\}$. For convenience of notation in the subsequent discussion, for every element $\mathbf{x} \in \mathbf{X}$ we abbreviate the operator defined in (3) and (4) by $L : \mathbf{X} \to \mathbf{Y}$ where

$$\mathbf{X} = \mathbb{R}^m \times \prod_{i=1}^n U_i \qquad \text{and} \qquad \mathbf{Y} = \mathbb{R}^m \times \prod_{i=1}^n V_i \tag{42}$$

with the assumption that $V_i \subset \overline{\mathcal{H}}^{-2}$ also has the complete orthogonal set $\{\varphi_k : k \in \mathcal{J}_i\}$. This is the most general form of the operator L, and standard results imply that L is a bounded linear operator $L \in \mathcal{L}(\mathbf{X}, \mathbf{Y})$.

As mentioned earlier, the constructive implicit function theorem crucially relies on being able to find a bound K such that $\|L^{-1}\|_{\mathcal{L}(\mathbf{Y},\mathbf{X})} \leq K$. Our goal is to accomplish this by using a finite-dimensional approximation for L, since that can be analyzed via rigorous computational means. Our finite-dimensional approximation for L is given as follows. For fixed $N \in \mathbb{N}$ define the finite-dimensional spaces

$$\mathbf{X}_N = P_N \mathbf{X} \qquad \text{and} \qquad \mathbf{Y}_N = P_N \mathbf{Y}\,,$$

where the projection operator given in (30) is applied componentwise on the functional components of $\mathbf{X}$, $\mathbf{Y}$, i.e., on each U_i individually, and acts as the identity on the scalar components. We then define $L_N : \mathbf{X}_N \to \mathbf{Y}_N$ by

$$L_N = P_N L|_{\mathbf{X}_N}\,. \tag{43}$$

Let K_N be a bound on the inverse of the finite-dimensional operator L_N, i.e., suppose that we have established the estimate

$$\left\|L_N^{-1}\right\|_{\mathcal{L}(\mathbf{Y}_N,\mathbf{X}_N)} \leq K_N\,, \tag{44}$$

where the spaces $\mathbf{X}_N$ and $\mathbf{Y}_N$ are equipped with the norms of $\mathbf{X}$ and $\mathbf{Y}$, respectively. We will discuss further details on appropriate coordinate systems and the actual computation of both L_N and K_N in Section 4.2. Nevertheless, after these preparations we are able to state our main result for this section.

Theorem 4.1 (*Inverse Estimate for Fourth-Order Operators*)**.** *Consider the spaces* $\mathbf{X}$ *and* $\mathbf{Y}$ *defined in* (42)*, as well as the bounded linear operator* $L \in \mathcal{L}(\mathbf{X}, \mathbf{Y})$ *acting on* $m \in \mathbb{N}_0$ *scalar parameters* $\eta_1, \ldots, \eta_m$ *and on* $n \in \mathbb{N}$ *functions* $v_k : \Omega \to \mathbb{R}$ *in such a way that the first* m *components of* L *are given by the scalars*

$$\sum_{i=1}^m \alpha_{ki}\eta_i + \sum_{j=1}^n l_{kj}(v_j) \qquad \text{for} \qquad k = 1, \ldots, m\,, \tag{45}$$

and the next n *components of* L *are given by the functions*

$$-\beta_k \Delta^2 v_k - \sum_{i=1}^m b_{ki}\eta_i - \Delta \sum_{j=1}^n c_{kj} v_j - \sum_{j=1}^n \gamma_{kj} v_j \qquad \text{for} \qquad k = 1, \ldots, n. \tag{46}$$

In these formulas, the variables $\alpha_{ki} \in \mathbb{R}$*,* $\beta_k > 0$*, and* $\gamma_{kj} \in \mathbb{R}$ *are real constants, while* $b_{ki} \in \overline{\mathcal{H}}^0$*, and* $c_{kj} \in \mathcal{H}^2$*. Moreover, the* l_{kj} *denote bounded linear functionals with Riesz representative in the spaces* $P_N U_j$*, i.e., there exist functions* $a_{kj} \in P_N U_j$ *such that one has the identities* $\ell_{kj}(v_j) = (a_{kj}, v_j)_{\overline{\mathcal{H}}^2}$*.*

Let K_N *be a constant satisfying* (44)*, and define* $C_T = (\min_{j=1,\ldots,n} \beta_j)^{-1} > 0$*. Furthermore, define the constants* A *and* B *by*

$$A \coloneqq \frac{K_N\sqrt{n}}{\pi^2 N^2} \left(\sum_{k=1}^n \max_{1\leq j\leq n} \|c_{kj}\|_\infty^2 \right)^{1/2},$$

$$B \coloneqq \frac{C_T\sqrt{2\max\{m,n\}}}{\pi^2 N^2} \left(\sum_{k=1}^n \max_{\substack{1\leq i\leq m \\ 1\leq j\leq n}} \left\{ \|b_{ki}\|_{\overline{\mathcal{H}}^0}, \left(C_b C_e \|c_{kj}\|_{\mathcal{H}^2} + \frac{|\gamma_{kj}|}{\pi^2} \right) \right\}^2 \right)^{1/2},$$

and assume there exists a constant $\tau > 0$ *and an integer* $N \in \mathbb{N}$ *such that*

$$\sqrt{A^2 + B^2} \;\leq\; \tau \;<\; 1. \tag{47}$$

Then the operator L *in* (42) *satisfies*

$$\left\|L^{-1}\right\|_{\mathcal{L}(\mathbf{Y},\mathbf{X})} \leq \frac{\max(K_N, C_T)}{1-\tau}\,. \tag{48}$$

At first glance it might seem strange that the constants α_{kj} and the functions a_{kj} do not enter either the condition in (47) or the estimate in (48). This, however, is not true, as they determine the constant K_N from (44).

Before we begin to prove this main theorem, we state a necessary result which is based on a Neumann series argument to derive bounds on the operator norm of an inverse of an operator. This is a standard functional-analytic technique, which we state here for the reader's convenience. A proof can be found in [25, Lemma 4].

Proposition 4.2 (*Neumann Series Inverse Estimate*)**.** *Let $\mathcal{A} \in \mathcal{L}(\mathbf{X}, \mathbf{Y})$ be an arbitrary bounded linear operator between two Banach spaces, and let $\mathcal{S} \in \mathcal{L}(\mathbf{Y}, \mathbf{X})$ be one-to-one. Assume that there exist positive constants ϱ_1 and ϱ_2 such that*

$$\|I - \mathcal{S}\mathcal{A}\|_{\mathcal{L}(\mathbf{X},\mathbf{X})} \leq \varrho_1 < 1 \qquad \text{and} \qquad \|\mathcal{S}\|_{\mathcal{L}(\mathbf{Y},\mathbf{X})} \leq \varrho_2 \ .$$

Then $\mathcal{A}$ is one-to-one and onto, and

$$\|\mathcal{A}^{-1}\|_{\mathcal{L}(\mathbf{Y},\mathbf{X})} \leq \frac{\varrho_2}{1-\varrho_1} \ .$$

In subsequent discussions, we will refer to $\mathcal{S}$ as an approximate inverse*.*

We are now ready to proceed with the proof of the main result of the section, Theorem 4.1. Our goal is to prove that L is one-to-one, onto, and has an inverse whose operator norm is bounded by the value

$$K = \frac{\max(K_N, C_T)}{1-\tau} \ .$$

The complete proof of the above is spread across the remaining subsections, with the following structure of the key definitions and auxiliary results:

- Section 4.2, Lemma 4.3 provides a computable upper bound for $\left\|L_N^{-1}\right\|$.
- Section 4.3, Definition 4.5 gives a construction of the approximate inverse $\mathcal{S}$.
- Section 4.3, Lemma 4.6 shows that we can take $\varrho_2 = \max(K_N, C_T)$.
- Section 4.4, Lemma 4.8 provides a formula for ϱ_1.

Once all of these results have been established, the proof of Theorem 4.1 is complete.

4.2. Finite-dimensional projections of the linearization

In this section, we consider L_N, the finite-dimensional projection of the operator L, which was introduced in (43). The linear map L_N is tractable using rigorous computational methods, since calculating a finite-dimensional inverse is something that can be done using numerical linear algebra. To derive L_N in more detail, we recall the definitions of the following projection spaces, all of which are Hilbert spaces:

$$\begin{aligned} \mathbf{X} &= \mathbb{R}^m \times \textstyle\prod_{i=1}^n U_i \ , & \mathbf{X}_N &= P_N\mathbf{X} \ , & \mathbf{X}_\infty &= (I-P_N)\mathbf{X} \ , \\ \mathbf{Y} &= \mathbb{R}^m \times \textstyle\prod_{i=1}^n V_i \ , & \mathbf{Y}_N &= P_N\mathbf{Y} \ , & \mathbf{Y}_\infty &= (I-P_N)\mathbf{Y} \ , \end{aligned}$$

where the projection operator P_N is applied componentwise on the functional components of the spaces $\mathbf{X}$ and $\mathbf{Y}$, i.e., on each U_i individually, and acts as the identity on the scalar components. Recall that in (43) we defined $L_N : \mathbf{X}_N \to \mathbf{Y}_N$ via $L_N = P_N L|_{\mathbf{X}_N}$.

In order to work with this finite-dimensional operator in a straightforward computational manner, we need to find its matrix representation. If we define $(\mathcal{J}_i)_N$ to be the subset of all multi-indices $k \in \mathcal{J}_i$ such that $0 < |k|_\infty < N$ and $\mathcal{J}_N = \{(\mathcal{J}_1)_N, (\mathcal{J}_2)_N, \ldots, (\mathcal{J}_n)_N\}$, then both $\mathbf{X}_N$ and $\mathbf{Y}_N$ have the basis $\mathcal{B}_{\mathcal{J}_N}$ and one obtains the matrix representation B via the definition

$$B = \begin{pmatrix} B_{00} & B_{01} & \cdots & B_{0n} \\ B_{10} & B_{11} & \ddots & \vdots \\ \vdots & \ddots & \ddots & B_{(n-1)n} \\ B_{n0} & \cdots & B_{n(n-1)} & B_{nn} \end{pmatrix} \ , \tag{49}$$

where the matrices $B_{i,j}$ are as follows. Denote the element $\mathbf{x} \in \mathbf{X}$ in the form $\mathbf{x} = (\eta, v)$, where $\eta = (\eta_1, \eta_2, \ldots, \eta_m) \in \mathbb{R}^m$ and $v = (v_1, v_2, \ldots, v_n) \in \prod_{i=1}^n U_i$. Then the basis elements of $\mathcal{B}_{\mathcal{J}_N}$ are given by $(e_\ell, 0)$ for $1 \leq \ell \leq m$ and $(0, \Phi_{ik})$ for $k \in (\mathcal{J}_i)_N$ and $1 \leq i \leq n$, where Φ_{ik} is defined as the n-dimensional vector with φ_k in the i-th component and 0 elsewhere. In addition, we consider the Hilbert space $Z = \mathbb{R}^m \times (L^2(\Omega))^n$ and recall that for $t_1, t_2 \in \mathbb{R}^m$ and $w_1, w_2 \in \prod_{i=1}^n U_i$ the inner product on Z is defined via

$$((t_1, w_1), (t_2, w_2))_Z = (t_1, t_2)_{\mathbb{R}^m} + \sum_{i=1}^n ((w_1)_i, (w_2)_i)_{L^2(\Omega)} \ .$$

Then the above matrices B_{ij} are defined via the identities

$$\begin{aligned}
(B_{00})_{k\ell} &= (L[(e_\ell, 0)], (e_k, 0))_Z \ , && k = 1, \dots, m \ , && \ell = 1, \dots, m \ , \\
(B_{i0})_{k\ell} &= (L[(e_\ell, 0)], (0, \Phi_{ik}))_Z \ , && k \in (\mathcal{J}_i)_N \ , && \ell = 1, \dots, m \ , \\
(B_{0j})_{k\ell} &= (L[(0, \Phi_{j\ell})], (e_k, 0))_Z \ , && k = 1, \dots, m \ , && \ell \in (\mathcal{J}_j)_N \ , \\
(B_{ij})_{k\ell} &= (L[(0, \Phi_{j\ell})], (0, \Phi_{ik}))_Z \ , && k \in (\mathcal{J}_i)_N \ , && \ell \in (\mathcal{J}_j)_N \ ,
\end{aligned}$$

where $i, j = 1, \dots, n$. To conclude the abstract definition, we emphasize that

$$\begin{aligned}
B_{00} &\in \mathbb{R}^{m\times m} \ , && B_{0j} \in \mathbb{R}^{m\times \#(\mathcal{J}_j)_N} \ , \\
B_{i0} &\in \mathbb{R}^{\#(\mathcal{J}_i)_N \times m} \ , && B_{ij} \in \mathbb{R}^{\#(\mathcal{J}_i)_N \times \#(\mathcal{J}_j)_N} \ ,
\end{aligned}$$

where $\#S$ denotes the number of elements in the set S.

Now that we have properly defined the involved function spaces and the procedure to construct the matrix representation B of L_N, we can use (45) and (46) to obtain an explicit representation of L acting on $\mathbf{x} = (\eta, v) \in \mathbf{X}$. As mentioned in the formulation of Theorem 4.1, using the Riesz Representation theorem one can write each functional $\ell_{kj}(v_j)$ in (45) as the inner product $(a_{kj}, v_j)_{\overline{\mathcal{H}}^2}$. This substitution yields the explicit form

$$L\mathbf{x} = \begin{pmatrix} \left[\sum_{i=1}^m \alpha_{ki}\eta_i + \sum_{j=1}^n (a_{kj}, v_j)_{\overline{\mathcal{H}}^2}\right]_{k=1}^m \\ \left[-\beta_k \Delta^2 v_k - \sum_{i=1}^m b_{ki}\eta_i - \Delta \sum_{j=1}^n c_{kj} v_j - \sum_{j=1}^n \gamma_{kj} v_j\right]_{k=1}^n \end{pmatrix} , \tag{50}$$

which in turn leads to the following explicit forms for the components of B:

$$(B_{00})_{k\ell} = \alpha_{k\ell} \ , \tag{51a}$$

$$(B_{i0})_{k\ell} = -(b_{i\ell}, \varphi_k)_{L^2(\Omega)} \ , \tag{51b}$$

$$(B_{0j})_{k\ell} = (a_{kj}, \varphi_\ell)_{\overline{\mathcal{H}}^2} \ , \tag{51c}$$

$$\begin{aligned}
(B_{ij})_{k\ell} &= (-\delta_{ij}\beta_i \Delta^2 \varphi_\ell - \Delta c_{ij}\varphi_\ell - \gamma_{ij}\varphi_\ell, \varphi_k)_{L^2(\Omega)} \\
&= (-\delta_{ij}\beta_i \kappa_\ell^2 \varphi_\ell + \kappa_k c_{ij}\varphi_\ell - \gamma_{ij}\varphi_\ell, \varphi_k)_{L^2(\Omega)} \\
&= -\delta_{ij}\delta_{k\ell}\beta_i\kappa_\ell^2 - \gamma_{ij}\delta_{k\ell} + (\kappa_k c_{ij}\varphi_\ell, \varphi_k)_{L^2(\Omega)} \ ,
\end{aligned} \tag{51d}$$

where we use $(-\Delta c_{ij}\varphi_\ell, \varphi_k)_{L^2(\Omega)} = (c_{ij}\varphi_\ell, -\Delta\varphi_k)_{L^2(\Omega)} = (c_{ij}\varphi_\ell, \kappa_k\varphi_k)_{L^2(\Omega)}$, as well as (25).

The matrix representation B characterizes L_N on the algebraic level in the following sense. If we consider an element $\mathbf{x}_N \in \mathbf{X}_N$, then one can introduce the representations

$$\mathbf{x}_N = \sum_{b\in\mathcal{B}_{\mathcal{J}_N}} \xi_b b \qquad \text{and} \qquad L_N\mathbf{x}_N = \sum_{b\in\mathcal{B}_{\mathcal{J}_N}} \zeta_b b \ ,$$

where the coefficients satisfy both $\xi_b \in \mathbb{R}$ and $\zeta_b \in \mathbb{R}$, and the basis elements b are taken from the set

$$\mathcal{B}_{\mathcal{J}_N} = \left\{ e_j \times 0_{\left(\overline{\mathcal{H}}^2\right)^n} \right\}_{j=1\dots m} \bigcup \left\{ 0_{\mathbb{R}^m \times \left(\overline{\mathcal{H}}^2\right)^{i-1}} \times \varphi_k \times 0_{\left(\overline{\mathcal{H}}^2\right)^{n-i}} \right\}_{i=1\dots n,\ k\in(\mathcal{J}_i)_N} .$$

If we collect the numbers ξ_b and ζ_b in vectors ξ and ζ in the straightforward way, then one immediately obtains the matrix–vector identity

$$\zeta = B\xi \ .$$

This natural algebraic representation has one slight drawback that still needs to be addressed. We would like to use the regular Euclidean norm on real vector spaces, as well as the induced matrix norm, to study the $\mathcal{L}(\mathbf{X}_N, \mathbf{Y}_N)$-norm of L_N. For our computer-assisted proof, we are therefore interested in a scaled version of B which gives a computable K_N, and this scaled matrix is the subject of the following Lemma.

Lemma 4.3 (*Computable K_N*). *Let B be defined as in (49), $D_i = \mathrm{diag}\,(\{\kappa_k : k \in (\mathcal{J}_i)_N\})$, and let I_m be the $m \times m$ identity matrix. Assemble D as the block diagonal matrix*

$$D = \begin{pmatrix} I_m & 0 & 0 & \dots & 0 \\ 0 & D_1 & 0 & \dots & 0 \\ 0 & 0 & D_2 & \ddots & \vdots \\ \vdots & \vdots & \ddots & \ddots & 0 \\ 0 & 0 & \dots & 0 & D_n \end{pmatrix} ,$$

and define $\tilde{B} = D^{-1}BD^{-1}$. Then K_N in (44) can be taken as $\|\tilde{B}^{-1}\|_2$. In other words, using this formula, we can use interval arithmetic to establish a rigorous upper bound on the norm of this finite-dimensional inverse.

Proof. To begin with, we recall Lemma 3.1 which shows that, for each $i = 1, \dots, n$, the collection $\{\kappa_k^{-1}\varphi_k(x)\}$ with $k \in (\mathcal{J}_i)_N$ as above is an orthonormal basis in $P_N U_i \subset \overline{\mathcal{H}}^2$, and $\{\kappa_k\varphi_k(x)\}$ is an orthonormal basis in $\mathbf{Y}_N \subset \mathbf{Y}$, where the eigenvalues κ_k are defined in (25). Thus, we need to use the modified representations

$$\mathbf{x}_N = \sum_{\tilde{b}\in\tilde{\mathcal{B}}_{\mathcal{J}_N}} \tilde{\xi}_{\tilde{b}}\tilde{b} \qquad \text{and} \qquad L_N\mathbf{x}_N = \sum_{\hat{b}\in\hat{\mathcal{B}}_{\mathcal{J}_N}} \tilde{\zeta}_{\hat{b}}\hat{b}$$

where we use the alternative basis sets (note the $\kappa_k^{\pm 1}$ factors)

$$\tilde{\mathcal{B}}_{\mathcal{J}_N} = \left\{ e_j \times 0_{\left(\overline{\mathcal{H}}^2\right)^n} \right\}_{j=1\dots m} \bigcup \left\{ 0_{\mathbb{R}^m \times \left(\overline{\mathcal{H}}^2\right)^{i-1}} \times \kappa_k^{-1}\varphi_k \times 0_{\left(\overline{\mathcal{H}}^2\right)^{n-i}} \right\}_{i=1\dots n,\ k\in(\mathcal{J}_i)_N},$$

$$\hat{\mathcal{B}}_{\mathcal{J}_N} = \left\{ e_j \times 0_{\left(\overline{\mathcal{H}}^2\right)^n} \right\}_{j=1\dots m} \bigcup \left\{ 0_{\mathbb{R}^m \times \left(\overline{\mathcal{H}}^2\right)^{i-1}} \times \kappa_k\varphi_k \times 0_{\left(\overline{\mathcal{H}}^2\right)^{n-i}} \right\}_{i=1\dots n,\ k\in(\mathcal{J}_i)_N}.$$

In order to pass back and forth between these two representations we use the block diagonal matrix D. One can see that on the level of vectors we have

$$\xi = D^{-1}\tilde{\xi} \quad \text{and} \quad \zeta = D\tilde{\zeta}\,, \quad \text{and therefore} \quad \tilde{\zeta} = D^{-1}BD^{-1}\tilde{\xi}\,.$$

In view of Lemma 3.1 one then obtains

$$\|L_N\|_{\mathcal{L}(\mathbf{X}_N,\mathbf{Y}_N)} = \|\tilde{B}\|_2 \qquad \text{with} \qquad \tilde{B} = D^{-1}BD^{-1}\,,$$

where $\|\cdot\|_2$ denotes the regular induced 2-norm of a matrix. Moreover, one can verify that we also have the identity

$$\left\|L_N^{-1}\right\|_{\mathcal{L}(\mathbf{Y}_N,\mathbf{X}_N)} = \left\|\tilde{B}^{-1}\right\|_2 \tag{52}$$

which completes the proof. □

Remark 4.4. Since D is a diagonal matrix we can construct $\tilde{B}$ directly via the formulas

$$(\tilde{B}_{00})_{k\ell} = \alpha_{k\ell}\,, \tag{53a}$$

$$(\tilde{B}_{i0})_{k\ell} = -\frac{(b_{i\ell},\,\varphi_k)_{L^2(\Omega)}}{\kappa_k}\,, \tag{53b}$$

$$(\tilde{B}_{0j})_{k\ell} = \frac{(a_{kj},\,\varphi_\ell)_{\overline{\mathcal{H}}^2}}{\kappa_\ell}\,, \tag{53c}$$

$$(\tilde{B}_{ij})_{k\ell} = -\delta_{ij}\delta_{k\ell}\beta_i - \frac{1}{\kappa_k^2}\delta_{k\ell}\gamma_{ij} + \frac{1}{\kappa_\ell}\left(c_{ij}\varphi_\ell,\,\varphi_k\right)_{L^2(\Omega)}. \tag{53d}$$

4.3. Construction of an approximate inverse

The crucial part in the derivation of our norm bound for the inverse of L is the application of Proposition 4.2. For this, we need to construct an approximate inverse of this operator. Since this construction must be explicit, we will approach it in two steps. The first has already been accomplished in the last section, where we considered a finite-dimensional projection of L, which can be inverted numerically. In this section, we complement this finite-dimensional part with a consideration of the infinite-dimensional complementary space. For this, we refer the reader again to the definition of the matrix representation B in (49) and (51). Since the finite-dimensional approximation is constructed using the projections P_N which make use of the low-wavenumber basis functions, one would expect that as $N \to \infty$ this representation leads to increasingly better approximations of the operator L. Note in particular that every entry $\left(B_{ij}\right)_{k\ell}$ in (51d) is the sum of three terms, where the first one and the last one depend on the Laplacian eigenvalues from (25). One can easily see that among these three terms the first one dominates as $\ell \to \infty$, and thus also as $N \to \infty$. Based on this observation, we now describe how to use the inverse of the first term on the infinite tail in order to complement the inverse of L_N.

To describe this procedure in more detail, consider an arbitrary element $\mathbf{y} \in \mathbf{Y}$. We decompose this element into its finite-dimensional part and infinite tail in the form

$$\mathbf{y} = \sum_{b\in\mathcal{B}_I} \zeta_b b = \mathbf{y}_N + \mathbf{y}_\infty \in \mathbf{Y}_N \oplus \mathbf{Y}_\infty\,,$$

where we define

$$\mathbf{Y}_N = P_N\mathbf{Y} \qquad \text{and} \qquad \mathbf{Y}_\infty = (I - P_N)\,\mathbf{Y}\,.$$

Using this representation we also have

$$\mathbf{y}_\infty \;=\; \sum_{j=1}^{n} \sum_{k\in\mathcal{J}_j\setminus(\mathcal{J}_j)_N} \zeta_{jk}\Phi_{jk}$$

which enables the following definition.

Definition 4.5 (*Approximate Inverse Operator*)**.** Let $\mathbf{y}_N, \mathbf{y}_\infty$ be as above. We define the operator $T : \mathbf{Y}_\infty \to \mathbf{X}_\infty$ as

$$T\mathbf{y}_\infty \;=\; T\sum_{j=1}^{n} \sum_{k\in\mathcal{J}_j\setminus(\mathcal{J}_j)_N} \zeta_{jk}\Phi_{jk} \;=\; -\sum_{j=1}^{n} \sum_{k\in\mathcal{J}_j\setminus(\mathcal{J}_j)_N} \frac{\zeta_{jk}}{\beta_j\kappa_k^2}\Phi_{jk}\,,$$

and the operator $S : \mathbf{Y} \to \mathbf{X}$ as

$$S\mathbf{y} \;=\; L_N^{-1}\mathbf{y}_N + T\mathbf{y}_\infty. \tag{54}$$

One can readily see that the operator $T = S|_{\mathbf{Y}_\infty}$ is one-to-one and onto, and the operator S is the candidate approximate inverse of $L \in \mathcal{L}(\mathbf{X}, \mathbf{Y})$.

To close this section, we now derive a bound on the operator norm of S, since this will be needed in the application of Proposition 4.2.

Lemma 4.6 (*Computable* ϱ_2)**.** *Consider the two operators S, T as defined in Definition 4.5, assume that $\beta_j > 0$ for $j = 1, \dots, n$, and define the constant $C_T = (\min_{j=1,\dots,n}\beta_j)^{-1} > 0$ as in Theorem 4.1. Then we have the two inequalities*

$$\|T\|_{\mathcal{L}(\mathbf{Y}_\infty,\mathbf{X}_\infty)} \le C_T \qquad \text{and} \qquad \|S\|_{\mathcal{L}(\mathbf{Y},\mathbf{X})} \le \max(K_N, C_T)\,,$$

where K_N was introduced in (44). Moreover, this implies that we may take $\varrho_2 = \max(K_N, C_T)$ in Proposition 4.2.

Proof. To begin with, we let $\mathbf{y}_\infty \in \mathbf{Y}_\infty$ be arbitrary and show that $\|T\mathbf{y}_\infty\|_{\mathbf{X}} \le C_T\|\mathbf{y}_\infty\|_{\mathbf{Y}}$. This follows readily from $\beta_j > 0$, Lemma 3.1, and (27), as well as the identities

$$\begin{aligned}
\|T\mathbf{y}_\infty\|_{\mathbf{X}}^2 &= \left\| \sum_{j=1}^{n} \sum_{k\in\mathcal{J}_j\setminus(\mathcal{J}_j)_N} \frac{\zeta_{jk}}{\beta_j\kappa_k^2}\Phi_{jk} \right\|_{\overline{\mathcal{H}}^2}^2 \\
&= \sum_{j=1}^{n} \sum_{k\in\mathcal{J}_j\setminus(\mathcal{J}_j)_N} \frac{\zeta_{jk}^2\kappa_k^2}{(\beta_j\kappa_k^2)^2} \;\le\; C_T^2 \sum_{j=1}^{n} \sum_{k\in\mathcal{J}_j\setminus(\mathcal{J}_j)_N} \kappa_k^{-2}\zeta_{jk}^2 \\
&= C_T^2 \left\| \sum_{j=1}^{n} \sum_{k\in\mathcal{J}_j\setminus(\mathcal{J}_j)_N} \zeta_{jk}\Phi_{jk} \right\|_{\overline{\mathcal{H}}^{-2}}^2 \;=\; C_T^2\,\|\mathbf{y}_\infty\|_{\mathbf{Y}}^2\,.
\end{aligned}$$

This estimate in turn implies for all $\mathbf{y} = \mathbf{y}_N + \mathbf{y}_\infty \in \mathbf{Y}_N \oplus \mathbf{Y}_\infty$ the inequality

$$\begin{aligned}
\|S\mathbf{y}\|_{\mathbf{X}}^2 &= \|L_N^{-1}\mathbf{y}_N\|_{\mathbf{X}}^2 + \|T\mathbf{y}_\infty\|_{\mathbf{X}}^2 \\
&\le \underbrace{\|L_N^{-1}\|_{\mathcal{L}(\mathbf{Y}_N,\mathbf{X}_N)}^2}_{\le K_N^2} \|\mathbf{y}_N\|_{\mathbf{Y}}^2 + C_T^2\|\mathbf{y}_\infty\|_{\mathbf{Y}}^2 \;\le\; \max(K_N, C_T)^2\|\mathbf{y}\|_{\mathbf{Y}}^2\,,
\end{aligned}$$

where we used the definition of K_N from (44). This completes the proof of the lemma. □

In other words, the operator norm of the approximate inverse S can be bounded in terms of the inverse bound for the finite-dimensional projection given in Lemma 4.3. Furthermore, it follows directly from the definition of S that this operator is one-to-one, as long as L_N is — and the latter can be established using interval arithmetic. We conclude by remarking that, in many cases, the constant C_T can be taken as 1 through proper scaling of the diffusion coefficients in the model formulation.

4.4. Assembling the final inverse estimate

In the last section we addressed two crucial aspects of Proposition 4.2. On the one hand, we provided an explicit construction for the approximate inverse $S \in \mathcal{L}(\mathbf{Y}, \mathbf{X})$ of L defined in (42). On the other hand, we derived an upper bound on the operator norm of S, which can be computed using the finite-dimensional projection L_N of L. This in turn provides the constant ϱ_2 in Proposition 4.2. In this final subsection, we focus on the constant ϱ_1, i.e., we derive an upper bound on the norm $\|I - SL\|_{\mathcal{L}(\mathbf{X},\mathbf{X})}$, and show how this bound can be made smaller than one. Altogether, this will complete the proof of the estimate for the constant K which bounds the operator norm of L^{-1}. As a first step, we present in the following lemma a decomposition of L in terms of L_N and T that will help handle the infinite tail estimates.

Lemma 4.7. *Let $L \in \mathcal{L}(\mathbf{X}, \mathbf{Y})$ be as in (50), and let $S \in \mathcal{L}(\mathbf{Y}, \mathbf{X})$, $T \in \mathcal{L}(\mathbf{Y}_\infty, \mathbf{X}_\infty)$ be as in Definition 4.5. Further, let P_N be as defined in (30) and $L_N \in \mathcal{L}(\mathbf{X}_N, \mathbf{Y}_N)$ be as in (43). Then, using the additive representation $\mathbf{x} = \mathbf{x}_N + \mathbf{x}_\infty = (\eta, P_N v) + (0, (I - P_N)v) \in \mathbf{X}_N \oplus \mathbf{X}_\infty$, we have the identity*

$$L\mathbf{x} = (L_N \mathbf{x}_N + \mathcal{M}\mathbf{x}_\infty) + \left(T^{-1}\mathbf{x}_\infty - \mathcal{N}\mathbf{x}\right) , \tag{55}$$

where we define $\mathcal{M}, \mathcal{N}$ by

$$\mathcal{M}\mathbf{x}_\infty = \left(\left[\sum_{j=1}^{n} (a_{kj}, (I - P_N)v_j)_{\overline{\mathcal{H}}^2} \right]_{k=1}^{m} , \left[-P_N \Delta \sum_{j=1}^{n} c_{kj}(I - P_N)v_j \right]_{k=1}^{n} \right) , \tag{56}$$

$$\mathcal{N}\mathbf{x} = \left(0, \left[(I - P_N) \left(\sum_{i=1}^{m} \eta_i b_{ki} + \Delta \sum_{j=1}^{n} c_{kj} v_j + \sum_{j=1}^{n} \gamma_{kj} v_j \right) \right]_{k=1}^{n} \right) . \tag{57}$$

Proof. Notice that $L_N \mathbf{x}_N$ and $\mathcal{M}\mathbf{x}_\infty$ are in the finite-dimensional space $\mathbf{Y}_N$, while $T^{-1}\mathbf{x}_\infty$ and $\mathcal{N}\mathbf{x}$ are in $\mathbf{Y}_\infty$. With this in mind, we detail the derivation of (55) as follows. We first note that Δ and P_N commute. Then the explicit form of $L_N \mathbf{x}_N = P_N L \mathbf{x}_N$ is:

$$L_N \mathbf{x}_N = \begin{pmatrix} \left[\sum_{i=1}^{m} \alpha_{ki}\eta_i + \sum_{j=1}^{n} (a_{kj}, P_N v_j)_{\overline{\mathcal{H}}^2} \right]_{k=1}^{m} \\ \left[-\beta_k \Delta^2 P_N v_k - \sum_{i=1}^{m} \eta_i P_N b_{ki} - P_N \Delta \sum_{j=1}^{n} c_{kj} P_N v_j - \sum_{j=1}^{n} \gamma_{kj} P_N v_j \right]_{k=1}^{n} \end{pmatrix} .$$

Next, we consider the difference $L\mathbf{x} - L_N \mathbf{x}_N$. The first m components are given by the scalars

$$\sum_{j=1}^{n} (a_{kj}, (I - P_N)v_j)_{\overline{\mathcal{H}}^2} \qquad \text{for} \qquad k = 1, \dots, m ,$$

and we compute the next n components term by term for clarity. The terms involving b_{ki} and γ_{kj} are straightforward since P_N is linear. The term involving Δ^2 is also straightforward since Δ^ℓ commutes with P_N. This leaves the term involving c_{kj}, which we can decompose using P_N as follows:

$$\begin{aligned} -\Delta \sum_{j=1}^{n} c_{kj} v_j = &- P_N \Delta \sum_{j=1}^{n} c_{kj} P_N v_j - P_N \Delta \sum_{j=1}^{n} c_{kj}(I - P_N)v_j \\ &- (I - P_N)\Delta \sum_{j=1}^{n} c_{kj} P_N v_j - (I - P_N)\Delta \sum_{j=1}^{n} c_{kj}(I - P_N)v_j . \end{aligned}$$

This immediately implies that

$$-\Delta \sum_{j=1}^{n} c_{kj} v_j + P_N \Delta \sum_{j=1}^{n} c_{kj} P_N v_j = -P_N \Delta \sum_{j=1}^{n} c_{kj}(I - P_N)v_j - (I - P_N)\Delta \sum_{j=1}^{n} c_{kj} v_j ,$$

and therefore that last n components of the difference $L\mathbf{x} - L_N \mathbf{x}_N$ are given explicitly by

$$\underbrace{-P_N \Delta \sum_{j=1}^{n} c_{kj}(I - P_N)v_j}_{(\mathcal{M}\mathbf{x}_\infty)_k} \overbrace{-\beta_k \Delta^2 (I - P_N)v_k}^{(T^{-1}\mathbf{x}_\infty)_k} \underbrace{- \sum_{i=1}^{m} \eta_i (I - P_N) b_{ki} - (I - P_N)\Delta \sum_{j=1}^{n} c_{kj} v_j - \sum_{j=1}^{n} \gamma_{kj}(I - P_N)v_j}_{-(\mathcal{N}\mathbf{x})_k}$$

for $k = 1, \dots, n$. Thus we have shown $L\mathbf{x} - L_N \mathbf{x}_N = \mathcal{M}\mathbf{x}_\infty + T^{-1}\mathbf{x}_\infty - \mathcal{N}\mathbf{x}$ and completed the proof. □

We now use the above representation (55) of the operator L which is split along the subspaces $\mathbf{Y}_N$ and $\mathbf{Y}_\infty$ to derive an expression for the infinite tail $I - SL \in \mathcal{L}(\mathbf{X}, \mathbf{X})$. More precisely, we have

$$(I - SL)\mathbf{x} = T\mathcal{N}\mathbf{x} - L_N^{-1}\mathcal{M}\mathbf{x}_\infty , \tag{58}$$

and this will be verified in detail below. Notice that in this representation, the first term lies in the complement $\mathbf{X}_\infty$, while the second term is contained in the finite-dimensional space $\mathbf{X}_N$. The identity in (58) follows from the definition of S in

Definition 4.5 and

$$\begin{aligned} S L \mathbf{x} &= L_N^{-1} L_N \mathbf{x}_N + L_N^{-1} \mathcal{M} \mathbf{x}_\infty + T\left(T^{-1}\mathbf{x}_\infty - \mathcal{N}\mathbf{x}\right) \\ &= \mathbf{x}_N + \mathbf{x}_\infty + L_N^{-1}\mathcal{M}\mathbf{x}_\infty - T\mathcal{N}\mathbf{x} \\ &= \mathbf{x} + L_N^{-1}\mathcal{M}\mathbf{x}_\infty - T\mathcal{N}\mathbf{x}. \end{aligned}$$

After these preparations, we can now show that the operator norm of $I - SL$ can be expected to be small for sufficiently large N. This will provide an estimate for the constant ϱ_1 in Proposition 4.2, and conclude the proof of Theorem 4.1. However, we pause here to remind the reader that, in principle, the Riesz representative a_{kj} could be a general element of $\overline{\mathcal{H}}^2$. As mentioned in the introduction, we restrict ourselves to the case where a_{kj} is an element of the finite-dimensional space $P_N U_j \subset U_j$, which implies that the first m components of $\mathcal{M}\mathbf{x}_\infty$ are in fact identically 0.

Lemma 4.8 (*Computable ϱ_1*). *Let T be as in Definition 4.5, $\mathcal{N}$ be as in (57), and b_{ki}, c_{kj}, γ_{kj} be as in Theorem 4.1. Suppose further that, just as in Theorem 4.1, the Riesz representative a_{kj} of ℓ_{kj} lies in $P_N U_j$. Define $C_T = (\min_{j=1,\dots,n}\beta_j)^{-1} > 0$ as in Theorem 4.1, K_N as in Lemma 4.3, and finally A and B by*

$$A := \frac{K_N\sqrt{n}}{\pi^2 N^2}\left(\sum_{k=1}^n \max_{1\le j\le n}\|c_{kj}\|_\infty^2\right)^{1/2},$$

$$B := \frac{C_T\sqrt{2\max\{m,n\}}}{\pi^2 N^2}\left(\sum_{k=1}^n \max_{\substack{1\le i\le m\\ 1\le j\le n}}\left\{\|b_{ki}\|_{\overline{\mathcal{H}}^0}, \left(C_b C_e \|c_{kj}\|_{\mathcal{H}^2} + \frac{|\gamma_{kj}|}{\pi^2}\right)\right\}^2\right)^{1/2}.$$

Then, $\left\|L_N^{-1}\mathcal{M}\mathbf{x}_\infty\right\|_{\mathbf{X}} \le A\|\mathbf{x}_\infty\|_{\mathbf{X}}$, $\|T\mathcal{N}\mathbf{x}_\infty\|_{\mathbf{X}} \le B\|\mathbf{x}\|_{\mathbf{X}}$, and $\|I - SL\|_{\mathcal{L}(\mathbf{X},\mathbf{X})} \le \sqrt{A^2+B^2}$. Furthermore, as long as there exists a τ such that $\sqrt{A^2+B^2} \le \tau < 1$, we can take $\varrho_1 = \tau$ in Proposition 4.2.

Proof. For brevity in the verification, we define

$$M_k := \max_{1\le j\le n}\|c_{kj}\|_\infty^2,$$

$$N_k := \max_{\substack{1\le i\le m\\ 1\le j\le n}}\left\{\|b_{ki}\|_{\overline{\mathcal{H}}^0}, \left(C_b C_e\|c_{kj}\|_{\mathcal{H}^2} + \frac{|\gamma_{kj}|}{\pi^2}\right)\right\}^2,$$

and verify the estimates as follows. First, since $\|L_N^{-1}\|_{\mathcal{L}(\mathbf{Y}_N,\mathbf{X}_N)} \le K_N$, we must find a bound of the form

$$\|\mathcal{M}\mathbf{x}_\infty\|_{\mathbf{Y}_N} \le C_{\mathcal{M}}\|\mathbf{x}_\infty\|_{\mathbf{X}}.$$

By the definition of $\mathcal{M}$, and since $a_{kj} \in P_N U_j$, we have

$$\|\mathcal{M}\mathbf{x}_\infty\|_{\mathbf{Y}_N}^2 = \sum_{k=1}^n \left\| -P_N \Delta \sum_{j=1}^n c_{kj}(I-P_N)v_j\right\|_{\overline{\mathcal{H}}^{-2}}^2.$$

Since P_N is an orthogonal projection and Δ is an isometry, see Lemma 3.3(a), we have the upper bound

$$\|\mathcal{M}\mathbf{x}_\infty\|_{\mathbf{Y}_N}^2 \le \sum_{k=1}^n \left\|\sum_{j=1}^n c_{kj}(I-P_N)v_j\right\|_{\overline{\mathcal{H}}^0}^2 \le \sum_{k=1}^n\left(\sum_{j=1}^n \left\|c_{kj}(I-P_N)v_j\right\|_{\overline{\mathcal{H}}^0}\right)^2.$$

Lemma 3.4 then yields

$$\|\mathcal{M}\mathbf{x}_\infty\|_{\mathbf{Y}_N}^2 \le \sum_{k=1}^n\left(\sum_{j=1}^n \frac{1}{\pi^2 N^2}\left\|c_{kj}\right\|_\infty \left\|(I-P_N)v_j\right\|_{\overline{\mathcal{H}}^2}\right)^2,$$

and factoring out the maximum coefficients gives

$$\|\mathcal{M}\mathbf{x}_\infty\|_{\mathbf{Y}_N}^2 \le \left(\frac{1}{\pi^4 N^4}\sum_{k=1}^n \max_{1\le j\le n}\left\|c_{kj}\right\|_\infty^2\right)\left(\sum_{j=1}^n \left\|(I-P_N)v_j\right\|_{\overline{\mathcal{H}}^2}\right)^2.$$

Finally, the Cauchy–Schwarz inequality yields

$$\|\mathcal{M}\mathbf{x}_\infty\|_{\mathbf{Y}_N}^2 \le \left(\frac{n}{\pi^4 N^4}\sum_{k=1}^n \max_{1\le j\le n}\left\|c_{kj}\right\|_\infty^2\right)\sum_{j=1}^n \left\|(I-P_N)v_j\right\|_{\overline{\mathcal{H}}^2}^2,$$

which is precisely

$$\|\mathcal{M}\mathbf{x}_\infty\|_{\mathbf{Y}_N}^2 \leq \frac{n}{\pi^4 N^4}\left(\sum_{k=1}^{n} M_k\right)\|\mathbf{x}_\infty\|_{\mathbf{X}}^2 = C_{\mathcal{M}}^2\,\|\mathbf{x}_\infty\|_{\mathbf{X}}^2 .$$

Therefore, we can take $A := K_N C_{\mathcal{M}}$.

Second, since $\|T\|_{\mathcal{L}(\mathbf{Y}_\infty,\mathbf{X}_\infty)} \leq C_T$, we must find a bound of the form

$$\|\mathcal{N}\mathbf{x}\|_{\mathbf{Y}} \leq C_{\mathcal{N}}\|\mathbf{x}\|_{\mathbf{X}}.$$

By the definition of $\mathcal{N}$, we have

$$\|\mathcal{N}\mathbf{x}\|_{\mathbf{Y}}^2 \;=\; \sum_{k=1}^{n}\left\|(I-P_N)\left(\sum_{i=1}^{m}\eta_i b_{ki} + \Delta\sum_{j=1}^{n} c_{kj}v_j + \sum_{j=1}^{n}\gamma_{kj}v_j\right)\right\|_{\overline{\mathcal{H}}^{-2}}^2 .$$

We can then split the $\overline{\mathcal{H}}^{-2}$-norm term with the triangle inequality and use Lemmas 3.2(c), 3.3(a), and 3.4 to obtain the upper bound

$$\|\mathcal{N}\mathbf{x}\|_{\mathbf{Y}}^2 \leq \sum_{k=1}^{n}\left(\sum_{i=1}^{m}\frac{|\eta_i|\,\|b_{ki}\|_{\overline{\mathcal{H}}^0}}{\pi^2N^2} + \sum_{j=1}^{n}\frac{\|c_{kj}v_j\|_{\mathcal{H}^2}}{\pi^2N^2} + \sum_{j=1}^{n}\frac{|\gamma_{kj}|\,\|v_j\|_{\overline{\mathcal{H}}^2}}{\pi^4N^4}\right)^2 .$$

Now, for the middle term involving c_{kj}, we use Lemma 3.2(b),(c) to obtain the upper bound

$$\|\mathcal{N}\mathbf{x}\|_{\mathbf{Y}}^2 \leq \sum_{k=1}^{n}\left(\sum_{i=1}^{m}\frac{|\eta_i|\,\|b_{ki}\|_{\overline{\mathcal{H}}^0}}{\pi^2N^2} + \sum_{j=1}^{n}\left[\frac{C_bC_e\|c_{kj}\|_{\mathcal{H}^2}\|v_j\|_{\overline{\mathcal{H}}^2}}{\pi^2N^2} + \frac{|\gamma_{kj}|\,\|v_j\|_{\overline{\mathcal{H}}^2}}{\pi^4N^4}\right]\right)^2 .$$

Noting that $N^{-4} \leq N^{-2}$ and applying the Cauchy–Schwarz inequality we find the upper bound

$$\|\mathcal{N}\mathbf{x}\|_{\mathbf{Y}}^2 \leq \frac{2}{\pi^4N^4}\sum_{k=1}^{n}\left(\left[\sum_{i=1}^{m}|\eta_i|\,\|b_{ki}\|_{\overline{\mathcal{H}}^0}\right]^2 + \left[\sum_{j=1}^{n}\left(C_bC_e\|c_{kj}\|_{\mathcal{H}^2} + \frac{|\gamma_{kj}|}{\pi^2}\right)\|v_j\|_{\overline{\mathcal{H}}^2}\right]^2\right).$$

Since we are aiming for a bound in terms of $\|\mathbf{x}\|_{\mathbf{X}}$, we factor out the maximum coefficients of $|\eta_i|$ and $\|v_j\|_{\overline{\mathcal{H}}^2}$, respectively, and can replace the right-hand side in the above bound by

$$\frac{2}{\pi^4N^4}\sum_{k=1}^{n}\left(\left[\max_{1\leq i\leq m}\|b_{ki}\|_{\overline{\mathcal{H}}^0}\sum_{i=1}^{m}|\eta_i|\right]^2 + \left[\max_{1\leq j\leq n}\left(C_bC_e\|c_{kj}\|_{\mathcal{H}^2} + \frac{|\gamma_{kj}|}{\pi^2}\right)\sum_{j=1}^{n}\|v_j\|_{\overline{\mathcal{H}}^2}\right]^2\right).$$

Note that the innermost sums are now independent of k, and we can repeat the previous step and apply the Cauchy–Schwarz inequality again to obtain the new bound

$$\|\mathcal{N}\mathbf{x}\|_{\mathbf{Y}}^2 \leq \frac{2}{\pi^4N^4}\left(\sum_{k=1}^{n}N_k\right)\left[m\sum_{i=1}^{m}|\eta_i|^2 + n\sum_{j=1}^{n}\|v_j\|_{\overline{\mathcal{H}}^2}^2\right],$$

from which $\|\mathcal{N}\mathbf{x}\|_{\mathbf{Y}} \leq C_{\mathcal{N}}\|\mathbf{x}\|_{\mathbf{X}}$ follows easily with

$$C_{\mathcal{N}} \;:=\; \frac{\sqrt{2\max\{m,n\}}}{\pi^2N^2}\left(\sum_{k=1}^{n}N_k\right)^{1/2} .$$

This concludes the proof of the second bound with $B := C_TC_{\mathcal{N}}$. The bound for $\|I - SL\|$ is a direct result of the bound derived here and Eq. (58). □

We also know from Lemma 4.6 that $\|S\|_{\mathcal{L}(\mathbf{Y},\mathbf{X})} \leq \max(K_N, C_T)$. Therefore, we can directly apply Proposition 4.2 with the constants $\varrho_1 = \sqrt{A^2+B^2} \leq \tau < 1$ and $\varrho_2 = \max(K_N, C_T)$, and this immediately implies that the operator L is one-to-one, onto, and the norm of its inverse operator is bounded via

$$\left\|L^{-1}\right\|_{\mathcal{L}(\mathbf{Y},\mathbf{X})} \;\leq\; \frac{\varrho_2}{1-\varrho_1} \;=\; \frac{\max(K_N, C_T)}{1-\tau} .$$

This completes the proof of Theorem 4.1.

5. Conclusions and future applications

In this paper, we have developed a framework for establishing a rigorous bound for the operator norm of the inverse of a general type of linear fourth-order elliptic operator that occurs in a large class of systems, such as for example in the context of materials science applications. We have then applied this framework to the triblock copolymer model, a three monomer version of the Ohta–Kawasaki equation. In particular, we have validated a series of equilibrium solutions in spatial dimensions one and two.

The strength of the constructions developed here are their flexibility. For example, with only minor modifications to the parameters, we have been able to use the same construction to validate pitchfork bifurcation points for the diblock copolymer equation [28]. Additionally, with relatively little additional effort, we will be able to use the same method for rigorous pseudo-arclength continuation methods for phase field materials models such as the Cahn–Hilliard, the Cahn–Morral, or the classical Ohta–Kawasaki systems. While we anticipate that there are still issues that will need to be addressed, such as incorporating preconditioning and sparseness into our construction, the generality of our approach means that as we address such considerations, one will not have to revisit them again for each separate system and dynamical question.

CRediT authorship contribution statement

Peter Rizzi: Conceptualization, Methodology, Formal analysis, Writing – original draft, Writing – review & editing, Software, Visualization. **Evelyn Sander:** Conceptualization, Methodology, Formal analysis, Writing – original draft, Writing – review & editing, Software, Visualization. **Thomas Wanner:** Conceptualization, Methodology, Formal analysis, Writing – original draft, Writing – review & editing, Software, Visualization.

Declaration of competing interest

The authors declare that they have no known competing financial interests or personal relationships that could have appeared to influence the work reported in this paper.

Data availability

The code will be posted on the publications web site of the third author math.gmu.edu/~wanner/.

Acknowledgments

The research of E.S. and T.W. was partially supported by the Simons Foundation, USA under Awards 636383 and 581334, respectively. We are thankful for the careful and useful comments of the anonymous referees.

References

[1] Ohta T, Kawasaki K. Equilibrium morphology of block copolymer melts. Macromolecules 1986;19:2621–32.
[2] van der Waals JD. The thermodynamic theory of capillarity flow under the hypothesis of a continuous variation in density. Verh Konink Akad Wetensch Amsterdam 1893;1:1–56.
[3] Bates FS, Fredrickson GH. Block copolymers–designer soft materials. Phys Today 1999;52:32–9.
[4] Nishiura Y. Far-from-Equilibrium Dynamics. Translations of Mathematical Monographs, vol. 209, Providence, RI: American Mathematical Society; 2002.
[5] Teramoto T, Nishiura Y. Morphological characterization of the diblock copolymer problem with topological computation. Jpn J Ind Appl Math 2010;27(2):175–90.
[6] Choksi R, Peletier MA, Williams JF. On the phase diagram for microphase separation of diblock copolymers: An approach via a nonlocal Cahn-Hilliard functional. SIAM J Appl Math 2009;69(6):1712–38.
[7] Cyranka J, Wanner T. Computer-assisted proof of heteroclinic connections in the one-dimensional Ohta-Kawasaki model. SIAM J Appl Dyn Syst 2018;17(1):694–731.
[8] Johnson I, Sander E, Wanner T. Branch interactions and long-term dynamics for the diblock copolymer model in one dimension. Discrete Contin Dyn Syst Ser A 2013;33(8):3671–705.
[9] Lessard J-P, Sander E, Wanner T. Rigorous continuation of bifurcation points in the diblock copolymer equation. J Comput Dyn 2017;4(1–2):71–118.
[10] Wanner T. Topological analysis of the diblock copolymer equation. In: Nishiura Y, Kotani M, editors. Mathematical challenges in a new phase of materials science. Springer Proceedings in Mathematics & Statistics, vol. 166, Springer-Verlag; 2016, p. 27–51.
[11] Ren X, Wei J. On energy minimizers of the diblock copolymer problem. Interfaces Free Bound 2003;5(2):193–238.
[12] Ren X, Wei J. Droplet solutions in the diblock copolymer problem with skewed monomer composition. Calc Var Partial Differential Equations 2006;25(3):333–59.
[13] Ren X, Wei J. Existence and stability of spherically layered solutions of the diblock copolymer equation. SIAM J Appl Math 2006;66(3):1080–99.
[14] Ren X, Wei J. Many droplet pattern in the cylindrical phase of diblock copolymer morphology. Rev Math Phys 2007;19(8):879–921.
[15] Cai S, Watanabe Y. A computer-assisted method for the diblock copolymer model. Z Angew Math Mech 2019;99(7). e201800125, 14.
[16] Sander E, Wanner T. Equilibrium validation in models for pattern formation based on Sobolev embeddings. Discrete Contin Dyn Syst Ser B 2021;26(1):603–32.

[17] van den Berg JB, Williams JF. Validation of the bifurcation diagram in the 2D Ohta-Kawasaki problem. Nonlinearity 2017;30(4):1584–638. http://dx.doi.org/10.1088/1361-6544/aa60e8.
[18] van den Berg JB, Williams JF. Rigorously computing symmetric stationary states of the Ohta-Kawasaki problem in three dimensions. SIAM J Math Anal 2019;51(1):131–58. http://dx.doi.org/10.1137/17M1155624.
[19] Wanner T. Computer-assisted equilibrium validation for the diblock copolymer model. Discrete Contin Dyn Sys Ser A 2017;37(2):1075–107.
[20] Nakazawa H, Ohta T. Microphase separation of ABC-type triblock copolymers. Macromolecules 1993;26(20):5503–11.
[21] Bohbot-Raviv Y, Wang Z-G. Discovering new ordered phases of block copolymers. Phys Rev Lett 2000;85:3428–31.
[22] Zheng W, Wang Z-G. Morphology of ABC triblock copolymers. Macromolecules 1995;28(21):7215–23.
[23] Ren X, Wang C. A stationary core-shell assembly in a ternary inhibitory system. Discrete Contin Dyn Syst Ser A 2017;37(2):983–1012.
[24] Wang C, Ren X, Zhao Y. Bubble assemblies in ternary systems with long range interaction. 2017, arXiv:1712.00724.
[25] Sander E, Wanner T. Validated saddle-node bifurcations and applications to lattice dynamical systems. SIAM J Appl Dyn Syst 2016;15(3):1690–733.
[26] Wanner T. Computer-assisted bifurcation diagram validation and applications in materials science. Proc Symp Appl Math 2018;74:123–74.
[27] Kamimoto S, Kim HK, Sander E, Wanner T. A computer-assisted study of red coral population dynamics. Pure Appl Funct Anal 2022;7(4). In press.
[28] Rizzi P, Sander E, Wanner T. Symmetry-induced pitchfork bifurcations in the diblock copolymer model. 2022, in preparation.
[29] Maier-Paape S, Stoth B, Wanner T. Spinodal decomposition for multi-component Cahn-Hilliard systems. J Stat Phys 2000;98(3–4):871–96.
[30] Desi JP, Edrees H, Price J, Sander E, Wanner T. The dynamics of nucleation in stochastic Cahn-Morral systems. SIAM J Appl Dyn Syst 2011;10(2):707–43.
[31] Maier-Paape S, Miller U, Mischaikow K, Wanner T. Rigorous numerics for the Cahn-Hilliard equation on the unit square. Rev Mat Complut 2008;21(2):351–426.
[32] Maier-Paape S, Mischaikow K, Wanner T. Structure of the attractor of the Cahn-Hilliard equation on a square. Int J Bifurcation Chaos 2007;17(4):1221–63.
[33] Elliott CM, Luckhaus S. A generalized diffusion equation for phase separation of a multi-component mixture with interfacial free energy. Preprint 195, Bonn: Sonderforschungsbereich 256; 1991.
[34] Eyre DJ. Cascades of spinodal decompositions in the ternary Cahn-Hilliard equations. In: Chen LQ, Fultz B, Cahn JW, Manning JR, Morral JE, Simmons JA, editors. Mathematics of microstructure evolution. The Minerals, Metals & Materials Society; 1996, p. 367–78.
[35] Plum M. Computer-assisted proofs for semilinear elliptic boundary value problems. Jpn J Ind Appl Math 2009;26(2–3):419–42.
[36] Doedel E. AUTO: a program for the automatic bifurcation analysis of autonomous systems. In: Proceedings of the tenth manitoba conference on numerical mathematics and computing, vol. I (Winnipeg, Man., 1980), vol. 30. 1981, p. 265–84,
[37] Rump SM. INTLAB - interval laboratory. In: Csendes T, editor. Developments in reliable computing. Dordrecht: Kluwer Academic Publishers; 1999, p. 77–104, http://www.ti3.tuhh.de/rump/.
[38] Wanner T. Validated bounds on embedding constants for Sobolev space Banach algebras. Math Methods Appl Sci 2018;41(18):9361–76.
[39] Adams RA, Fournier JJF. Sobolev spaces. Second ed.. Amsterdam: Elsevier/Academic Press; 2003.